J. Fluid Mech. (1997), *vol.* 342, *pp.* 199–229. Printed in the United Kingdom

A global investigation of solitary-wave solutions to a two-parameter model for water waves

By ALAN R. CHAMPNEYS[1] AND MARK D. GROVES[2]

[1]Department of Engineering Mathematics, University of Bristol, Bristol, BS8 1TR, UK

[2]Department of Mathematical Sciences, Loughborough University, Loughborough, LE11 3TU, UK

(Received 19 March 1996 and in revised form 15 January 1997)

The model equation

$$\tfrac{2}{15}r^{\mathrm{iv}} - br'' + ar + \tfrac{3}{2}r^2 - \tfrac{1}{2}(r')^2 + [rr']' = 0$$

arises as the equation for solitary-wave solutions to a fifth-order long-wave equation for gravity–capillary water waves. Being Hamiltonian, reversible and depending upon two parameters, it shares the structure of the full steady water-wave problem. Moreover, all known analytical results for local bifurcations of solitary-wave solutions to the full water-wave problem have precise counterparts for the model equation.

At the time of writing two major open problems for steady water waves are attracting particular attention. The first concerns the possible existence of solitary waves of elevation as local bifurcation phenomena in a particular parameter regime; the second, larger, issue is the determination of the global bifurcation picture for solitary waves. Given that the above equation is a good model for solitary waves of depression, it seems natural to study the above issues for this equation; they are comprehensively treated in this article.

The equation is found to have branches of solitary waves of elevation bifurcating from the trivial solution in the appropriate parameter regime, one of which is described by an explicit solution. Numerical and analytical investigations reveal a rich global bifurcation picture including multi-modal solitary waves of elevation and depression together with interactions between the two types of wave. There are also new orbit-flip bifurcations and associated multi-crested solitary waves with non-oscillatory tails.

1. Introduction

This article is concerned with homoclinic orbits of the fourth-order ordinary differential equation

$$\tfrac{2}{15}r^{\mathrm{iv}} - br'' + ar + \tfrac{3}{2}r^2 - \tfrac{1}{2}(r')^2 + [rr']' = 0, \tag{1.1}$$

in which a and b are real parameters. (In this paper 'homoclinic' always means 'homoclinic to the origin'.) These orbits represent solitary-wave solutions of the fifth-order equation

$$r_t + \tfrac{2}{15}r_{xxxxx} - br_{xxx} + 3rr_x + 2r_xr_{xx} + rr_{xxx} = 0 \tag{1.2}$$

which travel with velocity $-a$. Equation (1.2) arises as a weakly nonlinear long-wave approximation to the classical gravity–capillary water-wave problem, the full formulation of which depends upon the dimensionless quantities $\alpha = gh/c^2$ and

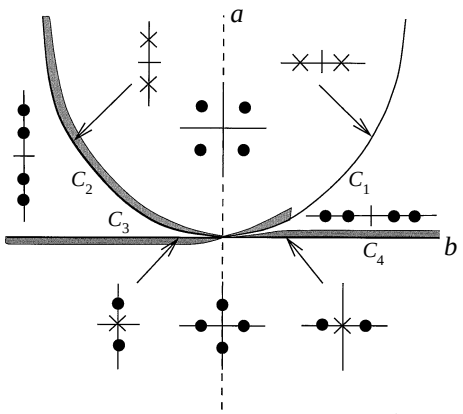

FIGURE 1. Eigenvalues in (b,a)-parameter space. The number of purely imaginary eigenvalues changes at $C_2 = \{(b,a) : a = 15b^2/8, b < 0\}$, $C_3 = \{(b,0) : b < 0\}$, $C_4 = \{(b,0) : b > 0\}$; at $C_1 = \{(b,a) : a = 15b^2/8, b > 0\}$ non-zero, real eigenvalues become complex without passing through zero. Dots and crosses denote respectively simple and double eigenvalues. The parameter regimes S_1, S_2, S_3, S_4 referred to in the text are the shaded regions near C_1, C_2, C_3, C_4, and $\mathscr{C}$ and $\mathscr{R}$ are the regions respectively above $C_1 \cup C_2$ and to the right of $C_1 \cup C_4$.

$\beta = \sigma/hc^2$. Here g is the acceleration due to gravity, h is the depth of the water in its undisturbed state, c is the speed of the wave and σ is the coefficient of surface tension (e.g. see Kirchgässner 1988). The long-wave approximation is derived by introducing small parameters ϵ and μ, which represent respectively a characteristic amplitude and wavenumber, writing $\epsilon = \mu^2$, $\alpha - 1 = a\mu^2$, $\beta - 1/3 = b$ and retaining terms up to $O(\mu^7)$ in a formal power-series expansion of the equations of motion (see Craig & Groves 1994 for a modern discussion of this approach). Although the formal derivation of (1.1) involves the assumption that b is not small (see Zufiria 1987, p. 187), equation (1.1) is of interest in its own right for all values of a and b and is here studied from this point of view.

The steady water-wave problem may be formulated as a reversible, infinite-dimensional, Hamiltonian dynamical system which depends upon the parameters α and β (Kirchgässner 1988; Iooss 1995; Groves & Toland 1997). Equation (1.1) has a similar structure: introducing real-valued variables

$$q_1 = r, \quad q_2 = r', \quad p_1 = -\tfrac{2}{15}r''' + br' - rr', \quad p_2 = \tfrac{2}{15}r'',$$

one may write it as the Hamiltonian system with energy

$$H = -\tfrac{1}{2}q_1^3 - \tfrac{1}{2}aq_1^2 + p_1q_2 - \tfrac{1}{2}bq_2^2 + \tfrac{15}{4}p_2^2 + \tfrac{1}{2}q_2^2q_1, \tag{1.3}$$

which is reversible under the transformation $t \mapsto -t$, $(q_1, q_2, p_1, p_2) \mapsto (q_1, -q_2, -p_1, p_2)$.

Let us now observe a further similarity between the two problems. The four eigenvalues λ of the linearization of the Hamiltonian system corresponding to (1.3) satisfy the equation

$$\tfrac{2}{15}\lambda^4 - b\lambda^2 + a = 0;$$

figure 1 shows how they depend upon the parameters a and b. Four eigenvalues in the countably infinite set of eigenvalues of the linearized steady water-wave problem depend upon α and β in a manner which is qualitatively similar to that shown in figure 1 (see Kirchgässner 1988, figure 1).

Local bifurcation phenomena for the full steady water-wave problem have been studied in the parameter regimes corresponding to those in figure 1. Amick & Kirchgässner (1989) studied the region corresponding to S_4 and found a unique small-amplitude solitary wave. This wave is a symmetric solitary wave of depression that decays exponentially and monotonically to zero at infinity, and corresponds to the wave found by Korteweg & deVries (1895) in the same parameter regime (Benjamin 1982). The region corresponding to S_2 was considered by Iooss & Kirchgässner (1990), Dias & Iooss (1993) and Iooss & Pérouème (1993). The combined work of these papers proves the existence of two modulated solitary waves whose envelopes are symmetric and decay exponentially to zero at infinity. The dominant feature of one wave is its central crest, while the dominant feature of the other is its central trough. This result has recently been considerably strengthened by Buffoni & Groves (1996), who showed that there are infinitely many geometrically distinct solitary waves in the parameter region S_3. Finally, Buffoni, Groves & Toland (1996*b*) considered the region corresponding to S_1 and showed that there are also infinitely many distinct solitary-wave solutions here. These *multi-modal* solutions are waves of depression which have an arbitrary but finite number of troughs, between which there are distributed smaller maxima and minima, and which have an exponentially decaying oscillatory tail at infinity. Section 2 below describes for the first time how analogous results may be obtained for the model equation (1.1).

Let us briefly mention the simpler equation

$$\tfrac{2}{15}r^{\mathrm{iv}} - br'' + ar + \tfrac{3}{2}r^2 = 0, \tag{1.4}$$

which is equivalent to the model equation studied by Zufiria (1987, equation (18)). This equation is obtained by introducing the scaled variables

$$\tilde{r} = \frac{r}{\epsilon^4}, \quad \tilde{t} = \epsilon t, \quad \tilde{a} = \frac{a}{\epsilon^4}, \quad \tilde{b} = \frac{b}{\epsilon^2}, \tag{1.5}$$

so that (1.1) becomes

$$\tfrac{2}{15}r^{\mathrm{iv}} - br'' + ar + \tfrac{3}{2}r^2 - \tfrac{1}{2}\epsilon^2(r')^2 + \epsilon^2[rr']' = 0, \tag{1.6}$$

and taking the limit $\epsilon \to 0$. Equation (1.4) is in fact equivalent to two one-parameter equations. Focusing on the case $a \neq 0$ and introducing the further transformation

$$u(T) = -\frac{3}{2|a|}r(t), \qquad T = \left(\frac{15|a|}{2}\right)^{1/4} t, \tag{1.7}$$

one finds that u satisfies one of the equations

$$u^{\mathrm{iv}} + P\ddot{u} + u - u^2 = 0, \tag{1.8}$$

$$u^{\mathrm{iv}} + P\ddot{u} - u - u^2 = 0, \tag{1.9}$$

in which $P = -b(15/2|a|)^{1/2}$, the dot denotes differentiation with respect to T and the equation is chosen so that the sign of the third term matches the sign of a. The curves C_1 and C_2 in figure 1 correspond respectively to $P = -2$ and $P = 2$ in (1.8), and the curves C_3 and C_4 correspond respectively to the limits $P \to \pm\infty$ in (1.8), (1.9). Bifurcation phenomena associated with equation (1.4) are therefore at most of codimension one. One must therefore add extra nonlinear terms to (1.4) to obtain an equation which is genuinely dependent upon two parameters; the $O(\epsilon^2)$ terms in (1.6) serve this purpose. Sections 3, 4 and 5 of the present paper are devoted to a global investigation of solitary-wave solutions to equation (1.1) as the two parameters a and b are varied; the main conclusions are presented in figure 26.

Section 3.1 contains an existence proof which shows that there is at least one solitary-wave solution in the parameter region $\mathscr{C} \cup \mathscr{R}$ and verifies the hypotheses required to apply the theory of Buffoni & Séré (1996), which asserts the existence of infinitely many solutions in the region $\mathscr{C}$. Numerically, these solutions are characterized as multi-modal waves of depression; their global bifurcation behaviour is investigated in §3.2. The numerical techniques used here, and throughout the remainder of the paper, are based upon a shooting method and continuation of solutions to a suitably truncated two-point boundary-value problem with the software package AUTO (Doedel & Kernevez 1986; Doedel, Keller & Kernevez 1991). The methods are robust and have been described in detail elsewhere (see Buffoni, Champneys & Toland 1996*a*; Champneys & Spence 1993 and the references therein).

In §4 attention is turned to the region S_3 in figure 1. The possibility of solitary-wave solutions to the full water-wave problem in the corresponding parameter regime was considered independently by Beale (1991) and Sun (1991) and elaborated upon by several others, notably Iooss & Kirchgässner (1992). These authors established the existence of *generalized solitary-wave solutions,* that is solutions homoclinic to periodic orbits. At the time of writing it remains unknown whether there are true solitary-wave solutions of the water-wave problem (solutions homoclinic to the origin) for the above parameter values. (Note however that Lombardi (1995) has shown that there are generalized solitary waves which decay at infinity to an oscillation of exponentially small amplitude.) For the model equation (1.1), numerical experiments presented in §4 indicate that a countable number of branches of solitary waves of elevation bifurcate from the trivial solution along the curve C_3 at the points $(b_n^-, 0)$, $n = 1, 2, \ldots$, where $0 > b_1^- > b_2^- > \cdots$. In fact the first branch is given by explicit formulae; the solution on this branch is an exact solution with the classical sech^2 profile. The solutions on the other branches have the same basic profile with an increasing number of small oscillations superimposed.

Section 5 examines global consequences of the existence of these branches of solitary waves of elevation. The branches all reach a turning point and enter the region $a > 0$ at $(b_n^+, 0)$, where $0 < b_1^+ < b_2^+ < \cdots$. In the region $\mathscr{R}$ they do not represent isolated solution curves but rather curves of solutions whose tails have a faster than expected exponential decay rate. Upon crossing such a curve in the parameter plane, one finds that solitary-wave solutions undergo an *orbit-flip bifurcation.* Various consequences of the orbit flip are examined: there is interaction between waves of elevation and depression; one can find infinitely many multi-modal waves of elevation in the region $\mathscr{C}$; and, most startlingly, there are countably infinite families of multi-crested solitary waves in the region $\mathscr{R}$, where the eigenvalues are real.

2. Local bifurcation phenomena

2.1. *The Korteweg–deVries solitary wave of depression*

Take $b > 0$ and $a = \mu$, where μ is a small positive number with $\mu < 15b^2/8$ (the region S_4 in figure 1), so that the linearized version of the Hamiltonian system corresponding to (1.3) has four real eigenvalues. When $\mu = 0$ there are two simple eigenvalues $-(15b/2)^{1/2}$, $(15b/2)^{1/2}$ with eigenvectors $\boldsymbol{v}_3$, $\boldsymbol{v}_4$ and a zero eigenvalue of geometric multiplicity 1 and algebraic multiplicity 2 with generalized eigenvectors $\boldsymbol{v}_1$, $\boldsymbol{v}_2$; here

$$\boldsymbol{v}_1 = \begin{pmatrix} 1 \\ 0 \\ 0 \\ 0 \end{pmatrix}, \quad \boldsymbol{v}_2 = \begin{pmatrix} 0 \\ 1 \\ b \\ 0 \end{pmatrix}, \quad \boldsymbol{v}_3 = \begin{pmatrix} 1/b \\ -(15/2b)^{1/2} \\ 0 \\ 1 \end{pmatrix}, \quad \boldsymbol{v}_4 = \begin{pmatrix} 1/b \\ (15/2b)^{1/2} \\ 0 \\ 1 \end{pmatrix}.$$

In terms of the new variables x_1, x_2, y_1, y_2 given by

$$(q_1, q_2, p_1, p_2)^T = x_1\boldsymbol{v}_1 + x_2\boldsymbol{v}_2 + y_1\boldsymbol{v}_3 + y_2\boldsymbol{v}_4,$$

one finds that the system becomes

$$x_1' = x_2 + \frac{x_1x_2}{b} + O(|(y_1, y_2)||(x_1, x_2, y_1, y_2)|), \tag{2.1}$$

$$x_2' = \frac{\mu x_1}{b} + \frac{3x_1^2}{2b} - \frac{x_2^2}{2b} + O(|(y_1, y_2)||(\mu, x_1, x_2, y_1, y_2)|), \tag{2.2}$$

$$y_1' = -\left(15b/2\right)^{1/2} y_1 + O(|(x_1, x_2, y_1, y_2)||(\mu, x_1, x_2, y_1, y_2)|), \tag{2.3}$$

$$y_2' = \left(15b/2\right)^{1/2} y_2 + O(|(x_1, x_2, y_1, y_2)||(\mu, x_1, x_2, y_1, y_2)|) \tag{2.4}$$

as $(\mu, x_1, x_2, y_1, y_2) \to 0$.

One may now use the *centre-manifold reduction theorem* for ordinary differential equations (see Iooss & Adelmeyer 1992), which asserts that for sufficiently small values of μ all small, bounded solutions of (2.1), (2.2), (2.3), (2.4) lie on a locally invariant, two-dimensional *centre manifold*

$$M_C^\mu = \{(x_1, x_2, y_1, y_2) : (y_1, y_2) = h(\mu, x_1, x_2)\},$$

where $h(\mu, x_1, x_2) = O(|(x_1, x_2)||(\mu, x_1, x_2)|)$ as $(\mu, x_1, x_2) \to 0$. Moreover, every solution of the reduced system obtained by writing $(y_1, y_2) = h(\mu, x_1, x_2)$ in (2.1), (2.2) generates a solution $(x_1, x_2, h(\mu, x_1, x_2))(t)$ of (2.1), (2.2), (2.3), (2.4). After the further change of variables

$$X_1(T) = \frac{x_1(t)}{\mu}, \quad X_2(T) = \frac{b^{1/2}x_2(t)}{\mu^{3/2}}, \quad T = \frac{\mu^{1/2}t}{b^{1/2}},$$

this reduced system is found to be

$$\dot{X}_1 = X_2 + O(\mu), \tag{2.5}$$

$$\dot{X}_2 = X_1 + \tfrac{3}{2}X_1^2 + O(\mu) \tag{2.6}$$

as $\mu \to 0$, in which a dot denotes differentiation with respect to T. It is a feature of the centre-manifold reduction that the reduced equations inherit the reversibility of the original dynamical system (Iooss & Adelmeyer 1992, §I.1.4), so that (2.5), (2.6) are reversible under the transformation $T \to -T$, $X_1 \to X_1$, $X_2 \to -X_2$. In the limit $\mu \to 0$, the system (2.5), (2.6) is equivalent to an ordinary differential equation for X_1, namely

$$\ddot{X}_1 = X_1 + \tfrac{3}{2}X_1^2,$$

which has the unique solitary-wave solution

$$X_1 = -\mathrm{sech}^2\left(\tfrac{1}{2}T\right).$$

This solution is a symmetric solitary wave of depression that decays monotonically and exponentially to zero as $T \to \pm\infty$. A straightforward application of the implicit-function theorem (cf. Kirchgässner 1988, Proposition 5.1) shows that the solution persists for small positive values of μ, in the sense that equations (2.5), (2.6), with any reversible $O(\mu)$ remainder terms, admit a solitary-wave solution $X_1(\mu, T)$ with the same properties.

2.2. *Envelope solitary waves*

Take $b = -d$, $a = 15d^2/8 + \mu$, where d is a positive real number and μ is small and positive (the region S_2 in figure 1), so that the linearized version of the Hamiltonian

system corresponding to (1.3) has four complex eigenvalues. When $\mu = 0$ there are two eigenvalues $\pm \mathrm{i}(15d/4)^{1/2}$ of geometric multiplicity 1 and algebraic multiplicity 2. The generalized eigenvectors are $\boldsymbol{v}_1$, $\boldsymbol{v}_2$ and $\bar{\boldsymbol{v}}_1$, $\bar{\boldsymbol{v}}_2$, where

$$\boldsymbol{v}_1 = \begin{pmatrix} -(1/2d)^{1/2} \\ -\mathrm{i}(15/8)^{1/2} \\ \mathrm{i}(15d^2/32)^{1/2} \\ (d/8)^{1/2} \end{pmatrix}, \qquad \boldsymbol{v}_2 = \begin{pmatrix} -\mathrm{i}(1/30d^2)^{1/2} \\ -(1/8d)^{1/2} \\ -(9d/32)^{1/2} \\ -\mathrm{i}(3/40)^{1/2} \end{pmatrix}.$$

Writing $(q_1, q_2, p_1, p_2)^T = z_1\boldsymbol{v}_1 + z_2\boldsymbol{v}_2 + \bar{z}_1\bar{\boldsymbol{v}}_1 + \bar{z}_2\bar{\boldsymbol{v}}_2$, one obtains the Hamiltonian system

$$z_1' = \frac{\partial H}{\partial \bar{z}_2}, \quad \bar{z}_1' = \frac{\partial H}{\partial z_2}, \quad z_2' = -\frac{\partial H}{\partial \bar{z}_1}, \quad \bar{z}_2' = -\frac{\partial H}{\partial z_1}, \tag{2.7}$$

where H is the original Hamiltonian expressed in terms of the variables $z_1, z_2, \bar{z}_1, \bar{z}_2$.

The next step is the use of normal-form theory developed by Elphick *et al.* (1987) and extended to Hamiltonian systems by Meyer & Hall (1992, Chap. VII). In the present setting, the theory states that there is a near identity, symplectic change of variable

$$z = Z + \Theta(Z, \mu),$$

where Θ is a polynomial of degree $n \geqslant 2$ in the variable (Z, μ) with the property that the transformed Hamiltonian takes the form

$$\tilde{H} = \tfrac{1}{2}\mathrm{i}(15d)^{1/2}(\bar{B}A - \bar{A}B) + B\bar{B} + \sum_{j=3}^{n+1} \tilde{H}_j(Z, \mu) + O(|Z|^2|(\mu, Z)|^n)$$

as $(Z, \mu) \to 0$. Here A, B, $\bar{A}$, $\bar{B}$ are the components of Z and the functions $\tilde{H}_j$, $j = 3, \ldots, n+1$ are polynomials which are homogeneous of degree j in (Z, μ) and are also real polynomial functions of $A\bar{A}$ and $\mathrm{i}(A\bar{B} - \bar{A}B)$ with coefficients that depend upon μ. Moreover $\tilde{H}_j(0, \mu) = 0$.

The above theory with $n = 3$ asserts that the transformed Hamiltonian is

$$\begin{aligned} H = {} & \tfrac{1}{2}\mathrm{i}(15d)^{1/2}(\bar{B}A - \bar{A}B) + B\bar{B} + \mu c_1 A\bar{A} + \mu \mathrm{i} c_2 A\bar{B} - \mu \mathrm{i} c_2 \bar{A}B \\ & + c_3 A^2\bar{A}^2 + \mathrm{i} c_4 A^2\bar{A}\bar{B} - \mathrm{i} c_4 A\bar{A}^2 B - c_5 A^2\bar{B}^2 + 2c_5 A\bar{A}B\bar{B} - c_5\bar{A}^2 B^2 \\ & + \mu^2 c_6 A\bar{A} + \mu^2 \mathrm{i} c_7 A\bar{B} - \mu^2 \mathrm{i} c_7 \bar{A}B + O(|Z|^2|(\mu, Z)|^3) \end{aligned}$$

as $(\mu, Z) \to 0$, where $c_1, \ldots, c_7$ are real constants. The theory below depends crucially on c_1 and c_3, which are readily obtained by directly computing the quadratic and cubic terms in Θ (see Iooss & Adelmeyer 1992). One finds that

$$c_1 = \frac{-1}{2d}, \qquad c_3 = \frac{19}{30d^4} - \frac{7}{4d^3} + \frac{45}{32d^2};$$

observe that c_1 is negative and c_3 is positive for all positive values of d.

Making the change of variables

$$A(t) = \mu^{1/2}\tilde{A}(\tilde{t})\exp(\mathrm{i}(15d/4)^{1/2}t), \quad B(t) = \mu\tilde{B}(\tilde{t})\exp(\mathrm{i}(15d/4)^{1/2}t), \quad \tilde{t} = \mu^{1/2}t$$

in Hamilton's equations one obtains the system

$$\dot{\tilde{A}} = \tilde{B} + O(\mu^{1/2}), \tag{2.8}$$

$$\dot{\tilde{B}} = -c_1\tilde{A} - 2c_3\tilde{A}|\tilde{A}|^2 + O(\mu^{1/2}) \tag{2.9}$$

as $\mu \to 0$. In the limit $\mu \to 0$, this system is equivalent to an ordinary differential

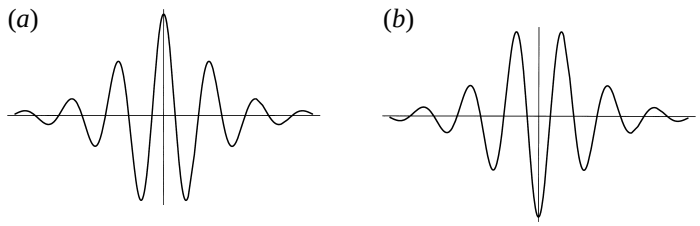

FIGURE 2. (*a*) Sketch of the envelope solitary wave of elevation; (*b*) sketch of the envelope solitary wave of depression.

equation for A, namely

$$\ddot{\tilde{A}} = -c_1\tilde{A} - 2c_3\tilde{A}|\tilde{A}|^2,$$

which has the family $\{\tilde{A}_\theta(t), \theta \in [0, 2\pi)\}$ of homoclinic solutions, where

$$\tilde{A}_\theta(\tilde{t}) = (-c_1/c_3)^{1/2}\mathrm{sech}((-c_1)^{1/2}\tilde{t})\exp(\mathrm{i}\theta).$$

Two of these homoclinic solutions, namely $\tilde{A}_0(\tilde{t})$ and $\tilde{A}_\pi(\tilde{t})$, are symmetric; they are respectively positive and negative functions of t that decay exponentially to zero as $\tilde{t} \to \infty$. An argument given by Iooss & Pérouème (1993, §IV.3) shows that both solutions persist for small positive values of μ, in the sense that equations (2.8), (2.9), with any $O(\mu^{1/2})$ remainder terms that are reversible under the transformation $t \to -t$, $(\tilde{A}, \tilde{B}, \bar{\tilde{A}}, \bar{\tilde{B}}) \to (\bar{\tilde{A}}, -\bar{\tilde{B}}, \tilde{A}, -\tilde{B})$, admit two homoclinic solutions $\tilde{A}_0(\mu, \tilde{t})$, $\tilde{A}_\pi(\mu, \tilde{t})$ with the same properties. The corresponding solutions of the model equation (1.1) are modulated solitary waves whose envelopes are symmetric and decay exponentially to zero at infinity. The dominant feature of one wave is its central crest, while the dominant feature of the other is its central trough; the waves are therefore termed *envelope solitary waves of elevation and depression*. They are sketched in figure 2.

2.3. *A plethora of solitary waves of depression*

Let us now consider the region of parameter space just to the right of the curve corresponding to C_1 in figure 1 and near and to the right of the point corresponding to $(b, a) = (0, 0)$ (the region S_1 in figure 1). Write

$$b = -\tfrac{2}{15}P\mu^2, \qquad a = \tfrac{2}{15}\mu^4,$$

where μ and P are real numbers and μ is small; the curve C_1 corresponds to $P = -2$. Introducing scaled variables

$$Q_1(T) = \frac{1}{\mu^4}q_1(t), \quad Q_2(T) = \frac{1}{\mu^5}q_2(t), \quad P_1(T) = \frac{1}{\mu^7}p_1(t), \quad P_2(T) = \frac{1}{\mu^6}p_2(t), \quad T = \mu t,$$

observe that the Hamiltonian system corresponding to (1.3) is transformed into the *Hamiltonian* system

$$\begin{pmatrix} \dot{Q}_1 \\ \dot{Q}_2 \\ \dot{P}_1 \\ \dot{P}_2 \end{pmatrix} = \begin{pmatrix} Q_2 \\ \frac{15}{2}P_2 \\ \frac{3}{2}Q_1^2 + \frac{2}{15}Q_1 \\ -P_1 - \frac{2}{15}PQ_2 \end{pmatrix} + O(\mu^2) \tag{2.10}$$

as $\mu \to 0$, where the dot denotes differentiation with respect to T. In the limit $\mu \to 0$

the system (2.10 is equivalent to an ordinary differential equation for Q_1, namely

$$Q_1^{\mathrm{iv}} + P\ddot{Q}_1 + Q_1 + \tfrac{45}{4}Q_1^2 = 0.$$

Writing $u = -45Q_1/4$, one finds that u satisfies equation (1.8).

Equation (1.8), which also arises as a model for nonlinear buckling of struts (Hunt, Bolt & Thompson 1989; Hunt & Wadee 1991), has been the subject of much recent study (see Amick & Toland 1992*a*,*b*; Iooss 1992; Champneys & Toland 1993; Buffoni 1993, 1995, 1996; Buffoni *et al.* 1996*a*; Buffoni & Séré 1996 and the references therein); the following results are of particular importance to the present investigation. Buffoni *et al.* (1996*a*, §2) showed that for $P \in (-\infty, -2]$ equation (1.8) has a positive, symmetric homoclinic solution which decays exponentially and monotonically to zero as $T \to \pm\infty$ and is the transverse intersection (relative to the zero-energy surface) of the stable and unstable manifolds of the zero equilibrium. Since transversality is an open condition, it follows that the same is true of the system (2.10) for $P \in (-2, -2+\epsilon_1)$ and sufficiently small μ, ϵ_1. With these values of P and μ, the system (2.10) is a four-dimensional Hamiltonian system which has four complex eigenvalues in its linearization and the work of Devaney (1976) therefore implies that there is a Smale horseshoe in the dynamics within the zero-energy surface. More specifically, there is a Poincaré map that has an invariant Cantor set upon which it is topologically conjugate to a full shift on a countably infinite set of symbols (see Wiggins 1988, pp. 275–286). Implicit in this construction is the existence of infinitely many homoclinic orbits which pass several times through a neighbourhood of the primary homoclinic orbit (see Belyakov & Shilnikov 1990). Consequently there are infinitely many distinct homoclinic solutions of (2.10) and hence of (1.1).

The homoclinic solutions of (1.8) are waves of elevation which have an arbitrary but finite number of large crests, between which there are distributed smaller local maxima and minima, and which have an exponentially decaying oscillatory tail at infinity. The set $\mathscr{H}$ of homoclinic orbits of (1.8) is divided into an infinite number of classes, each of which contains infinitely many distinct homoclinic solutions; the classes are characterized by the *modality,* that is the number of large crests, of their members and the waves within each class are classified by the number of small oscillations between their large crests. Using notation first introduced by Champneys & Toland (1993), one may assign a label $\boldsymbol{n}(\ell_1, \ldots, \ell_{n-1})$ to each homoclinic solution in $\mathscr{H}$. The solution labelled $\boldsymbol{n}(\ell_1, \ldots, \ell_{n-1})$ has modality n and the numbers ℓ_k, $k = 1, \ldots, n-1$, identify the solution within its class: it has $2[\ell_k/2]$ zeros and $2[(\ell_k - 1)/2] + 1$ local extrema between the kth and $(k+1)$th crests. (Here $[\cdot]$ denotes the integer part of a real number.) The uni-modal solution $\mathbf{1}()$ is termed the *primary* homoclinic solution. The homoclinic solutions of (2.10) and hence of (1.1) in the present parameter regime are classified in the same fashion. Notice, however, that they are waves of depression rather than elevation.

3. Solitary waves of depression – global phenomena

Before embarking upon an investigation of the global properties of solutions to (1.1) in the region $\mathscr{C}$, let us briefly summarize analogous results for the simpler equation (1.8) in the corresponding parameter region ($P \in (-2, 2)$).

The global bifurcation picture of homoclinic solutions to (1.8) for $P \in (-2, 2)$ has been studied analytically and numerically. Buffoni (1995) deduced that it admits infinitely many homoclinic solutions for each $P \in (-2, 2)$. Buffoni *et al.* (1996*a*) carried out extensive numerical investigations of equation (1.8) for $P \in (-2, 2)$ and found

that of all the branches of homoclinic solutions bifurcating at $P = -2$, only two continue through the range $P \in (-2, 2)$. (One may employ normal-form analysis of the type in §2.2 to show that (1.8) has two modulated solitary-wave solutions for $P \in (2 - \epsilon_2, 2)$, where ϵ_2 is a small, positive, real number (Grimshaw, Malomed & Benilov 1994).) Upon increasing P from $P = -2$, they found that every other branch reaches a turning point at a value $P^\star < 2$ of P (different for each branch) beyond which it ceases to exist. Decreasing P from this critical value, one may return to $P = -2$ along a different branch, arriving at $P = -2$ with an orbit of a different modality. One says that the two branches of homoclinic solutions *coalesce* at $P^\star$. Buffoni *et al.* (1996*a*, §4) support their numerical observations with geometric arguments concerning the intersection of the unstable manifold of the zero equilibrium and the symmetric section $\{(u, u', u'', u''') \in \mathbb{R}^4 : u' = u''' = 0\}$. These arguments have since been put on a rigorous mathematical footing by Knobloch (1994) for a general reversible or conservative dynamical system. Both papers conclude that a coalescence of two symmetric or asymmetric homoclinic orbits at a value $P^\star \in (-2, 2)$ of P is a codimension-one event, and that certain observed coalescences of asymmetric orbits are associated with bifurcations of two asymmetric orbits from a symmetric orbit.

3.1. *Critical-point theory*

Define a functional J on the Sobolev space $H^2(\mathbb{R})$ by the formula

$$J(r) = \frac{1}{2} \int_{\mathbb{R}} \left\{ \tfrac{2}{15} |r''|^2 + b|r'|^2 + ar^2 - rr'^2 + r^3 \right\} \mathrm{d}t \tag{3.1}$$

and observe that the homoclinic solutions of (1.1) are precisely the critical points of J, that is the points $r \in H^2(\mathbb{R})$ such that $J'(r) = 0$. For use in the theory below, let us note that

$$\langle J'(r), r \rangle = \int_{\mathbb{R}} \left\{ \tfrac{2}{15} |r''|^2 + b|r'|^2 + ar^2 - \tfrac{3}{2} rr'^2 + \tfrac{3}{2} r^3 \right\} \mathrm{d}t,$$

$$\langle J''(r)r, r \rangle = \int_{\mathbb{R}} \left\{ \tfrac{2}{15} |r''|^2 + b|r'|^2 + ar^2 - 3rr'^2 + 3r^3 \right\} \mathrm{d}t,$$

where $\langle \cdot, \cdot \rangle$ denotes the $H^2(\mathbb{R})$-inner product. One has the identities

$$\int_{\mathbb{R}} \left\{ \tfrac{2}{15} |r''|^2 + b|r'|^2 + ar^2 \right\} \mathrm{d}t = 6J(r) - 2\langle J'(r), r \rangle, \tag{3.2}$$

$$J(r) = \tfrac{1}{2} \langle J'(r), r \rangle - \tfrac{1}{4} K(r), \tag{3.3}$$

$$\langle J''(r)r, r \rangle = \langle J'(r), r \rangle + \tfrac{3}{2} K(r), \tag{3.4}$$

where

$$K(r) = \int_{\mathbb{R}} \left\{ -rr'^2 + r^3 \right\} \mathrm{d}t.$$

Let us begin by showing that 0 is a strict local minimum of J for values of a and b in the region $\mathscr{C} \cup \mathscr{R}$ in figure 1. Here the first step is to exhibit a positive constant c_1 such that

$$\int_{\mathbb{R}} \left\{ \tfrac{2}{15} |r''|^2 + b|r'|^2 + ar^2 \right\} \mathrm{d}t \geqslant c_1 \, \| r \|^2_{H^2(\mathbb{R})} .$$

For $a, b > 0$ one can take $c_1 = \min(2/15, b, a)$; to deal with the remaining case $a > 0$,

$-(8a/15)^{1/2} < b \leqslant 0$ observe that

$$\begin{aligned}\tfrac{2}{15}k^4+bk^2+a &= \tfrac{2}{15}k^4 + (2a/15)^{1/2}k^2 + a + \left[(15/2a)^{1/2}b - 1\right](2a/15)^{1/2}k^2 \\ &\geqslant \tfrac{2}{15}k^4 + (2a/15)^{1/2}k^2 + a + \tfrac{1}{3}\left[(15/2a)^{1/2}b - 1\right]\left[\tfrac{2}{15}k^4 + (2a/15)^{1/2}k^2 + a\right] \\ &= \tfrac{1}{3}\left[2 + (15/2a)^{1/2}b\right]\left[\tfrac{2}{15}k^4 + (2a/15)^{1/2}k^2 + a\right].\end{aligned}$$

It follows that

$$\begin{aligned}&\int_{\mathbb{R}} \left\{\tfrac{2}{15}|r''|^2 + b|r'|^2 + ar^2\right\} \mathrm{d}t \\ &= \int_{\mathbb{R}} \left\{\tfrac{2}{15}k^4 + bk^2 + a\right\} |\hat{r}|^2 \mathrm{d}k \\ &\geqslant \tfrac{1}{3}\left(2 + (15/2a)^{1/2}b\right) \int_{\mathbb{R}} \left\{\tfrac{2}{15}k^4 + (2a/15)^{1/2}k^2 + a\right\} |\hat{r}|^2 \mathrm{d}k \\ &= \tfrac{1}{3}\left(2 + (15/2a)^{1/2}b\right) \int_{\mathbb{R}} \left\{\tfrac{2}{15}|r''|^2 + (2a/15)^{1/2}|r'|^2 + ar^2\right\} \mathrm{d}t,\end{aligned}$$

where $\hat{r}$ denotes the Fourier transform of r, and one can take

$$c_1 = \tfrac{1}{3}\left(2 + (15/2a)^{1/2}b\right) \min\left(\tfrac{2}{15}, (2a/15)^{1/2}, a\right).$$

The estimates

$$\left|\int_{\mathbb{R}} r^3 \,\mathrm{d}t\right| \leqslant \int_{\mathbb{R}} |r|^3 \,\mathrm{d}t \leqslant c_2 \parallel r \parallel^3_{H^2(\mathbb{R})} \tag{3.5}$$

and

$$\begin{aligned}\left|\int_{\mathbb{R}} rr'^2 \,\mathrm{d}t\right| &\leqslant \int_{\mathbb{R}} |r|r'^2 \,\mathrm{d}t \\ &\leqslant \left(\int_{\mathbb{R}} r^2 \,\mathrm{d}t\right)^{1/2} \left(\int_{\mathbb{R}} r'^4 \,\mathrm{d}t\right)^{1/2} \\ &\leqslant c_3 \parallel r \parallel_{L^2(\mathbb{R})} \parallel r' \parallel^2_{H^1(\mathbb{R})} \\ &\leqslant c_3 \parallel r \parallel^3_{H^2(\mathbb{R})},\end{aligned} \tag{3.6}$$

where c_2, c_3 are positive constants, are obtained using the Cauchy–Schwarz inequality and the Sobolev embedding theorem. It follows from (3.5), (3.6) that the last two terms on the right-hand side of (3.1) are $O(\parallel r \parallel^3_{H^2(\mathbb{R})})$ as $r \to 0$, and one concludes that 0 is a strict local minimum of J for values of a and b satisfying $a > 0$, $b > -(8a/15)^{1/2}$.

Choosing $r \in H^2(\mathbb{R})$ such that $K(r) < 0$, one finds that

$$\lim_{s\to\infty} s^{-2}J(sr) = \lim_{s\to\infty} \left[\frac{1}{2}\int_{\mathbb{R}} \left\{\tfrac{2}{15}|r''|^2 + b|r'|^2 + ar^2\right\} \mathrm{d}t + \tfrac{1}{2}sK(r)\right] = -\infty.$$

The value of J on any ray $\{sr : s \in [0,\infty)\}$ with $K(r) < 0$ therefore initially increases from 0 before reaching a maximum and eventually becoming negative. Let Γ be the set of all paths whose images have this property, so that

$$\Gamma = \{\gamma \in C([0,1], H^2(\mathbb{R})) : \gamma(0) = 0, J(\gamma(1)) < 0\}.$$

The number

$$c = \inf_{\gamma\in\Gamma} \max_{s\in[0,1]} J(\gamma(s))$$

therefore represents the height of the 'lowest' path from 0 to a function which realizes a negative value of J. Notice that $c > 0$ because 0 is a strict local minimum of J. It follows from the *mountain-pass lemma* (Brezis & Nirenberg 1991, p. 943) that there is a *Palais–Smale sequence* $\{u_n\}$ such that $J(u_n) \to c$ and $J'(u_n) \to 0$ as $n \to \infty$. One may now apply a *concentration-compactness argument* along the lines of that given by Coti Zelati, Ekeland & Séré (1990) to deduce the existence of a non-trivial critical point $r^\star$ of J such that $J(r^\star) \leqslant c$. It follows that equation (1.1) has at least one homoclinic solution in the parameter region $\mathscr{C} \cup \mathscr{R}$.

The next step is to introduce the *natural-constraint manifold*

$$\begin{aligned} M &= \{r \in H^2(\mathbb{R}) : \langle J'(r), r\rangle = 0, K(r) < 0\} \\ &= \{r \in H^2(\mathbb{R}) : \langle J'(r), r\rangle = 0, J(r) > 0\}; \end{aligned}$$

here the first and second lines are equal because of (3.3). Equation (3.2) shows that all non-zero critical points r of J (in particular $r^\star$) satisfy $J(r) > 0$ and therefore lie on M. Now take any $r \in M$ and consider the path $h \in C([0,1], H^2(\mathbb{R}))$ given by $h(s) = Asr$ for a sufficiently large value of A. This path belongs to Γ, and the fact that $\langle J''(r)r, r\rangle < 0$ (see equation (3.4)) shows that $J(h(s))$ reaches a unique maximum at $s = 1/A$. It follows that $J(r) \geqslant c$ for all $r \in M$; in particular $J(r^\star) \geqslant c$. One concludes that $J(r^\star) = c$, so that $r^\star$ is a global minimizer of J on M.

The facts that $r^\star$ is the unique maximizer of J on the ray passing through $r^\star$ and that $r^\star$ is a global minimizer of J on M are precisely the hypotheses required to apply the theory of Buffoni & Séré (1996, pp. 290–293) in the parameter region $\mathscr{C}$. Under the additional hypothesis that $r^\star$ is isolated (up to time translations) in $H^2(\mathbb{R})$, the theory asserts the existence of a countably infinite family of *multi-bump* solutions. The nth member of this family resembles n copies of the primary orbit $r^\star$ separated by small-amplitude displacements and with exponentially decaying tails. Notice that if $r^\star$ is not isolated there must also be infinitely many distinct homoclinic solutions. In either case equation (1.1) has infinitely many geometrically distinct homoclinic solutions in the parameter region $\mathscr{C}$.

3.2. *Numerical computations*

Figure 3 depicts numerical computations of six symmetric homoclinic solutions to equation (1.1), namely the primary solution and the solutions labelled **2**(1) to **2**(5) for $a = 1$, $b = -0.5$. Notice that these parameter values are well away from the region S_1 in figure 1 where the theory of §2.3 applies. Figure 4 shows bifurcation diagrams for each solitary wave in figure 3; here b is fixed at $= -0.5$ and a is allowed to vary. Observe that only two waves, the primary and **2**(2) solutions, survive to reach the curve C_2 (at $a = 15/32$ for $b = -1/2$). The primary and **2**(2) solutions are depicted in figure 5 for a variety of values of a. (Here, and elsewhere in the remainder of this paper, such symmetric solitary waves are drawn only up to their point of symmetry; the origin of t is chosen for numerical convenience.) From figures 4 and 5 it is apparent that the amplitudes of both solutions decrease monotonically with a and reach zero at the curve C_2; in the vicinity of C_2 they are the envelope solitary waves described by the normal-form theory of §2.2. Every other solution branch reaches a limit point before reaching the curve C_2, where it coalesces with another branch.

Figures 6 and 7 show the behaviour of solutions on the **2**(1) and **2**(4) branches. As one follows the branches to their limit points and back along the second branch, the solutions begin to grow in amplitude again. In the case of the **2**(1) branch, a symmetrically related pair of oscillations develop into a secondary pair of troughs,

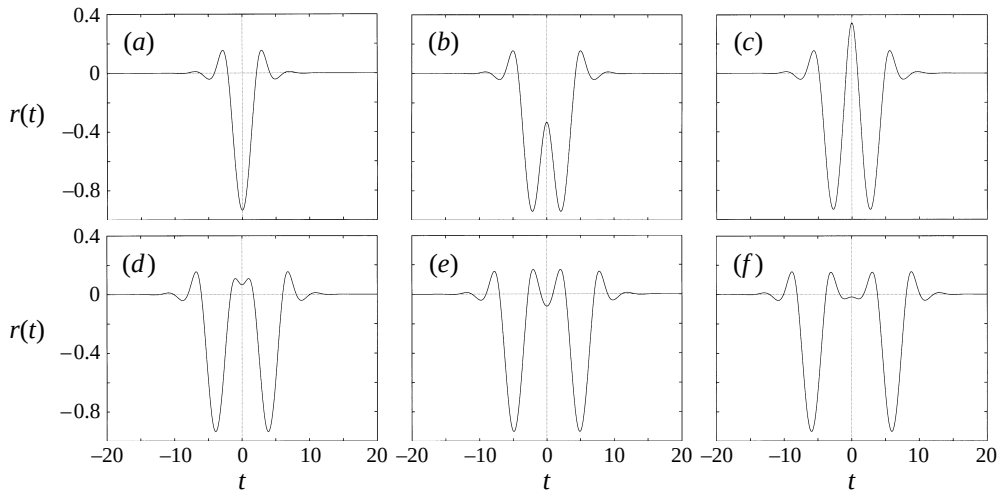

FIGURE 3. Primary and five bi-modal solitary waves for $a = 1$, $b = -0.5$: (*a*) primary; (*b*) **2**(1); (*c*) **2**(2); (*d*) **2**(3); (*e*) **2**(4); (*f*) **2**(5).

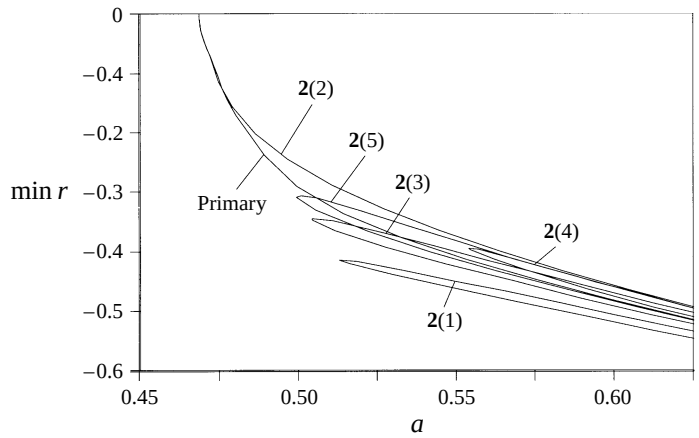

FIGURE 4. Bifurcation diagram with a of primary and five bi-modal solitary waves of depression for fixed $b = -0.5$.

so that the solution becomes a 4-modal orbit (figure 6*b*). Along the **2**(4) branch, the oscillation at the point of symmetry develops into a secondary trough, and the solution becomes a tri-modal orbit (figure 7*b*). The results presented in figures 4–7 are qualitatively the same as those found by Buffoni *et al.* (1996*a*) for equation (1.8), who also presented a detailed discussion of the rules governing which pairs of branches coalesce. These rules appear to be the same for the present equation, for which decreasing a corresponds to increasing P in equation (1.8). Numerical experiments for large values of a reveal no new behaviour. As a is increased, all troughs are observed to deepen indefinitely.

Figure 8 shows bifurcation diagrams for the same solitary waves when a is fixed (at 1) and b is allowed to vary. As b is increased, one obtains behaviour which is qualitatively similar to that shown in figure 4. Only two waves, the primary and **2**(2) solutions, survive to reach the curve C_2 (at $b = -(8/15)^{1/2}$ for $a = 1$). Every other solution branch reaches a limit point before reaching C_2, where it coalesces

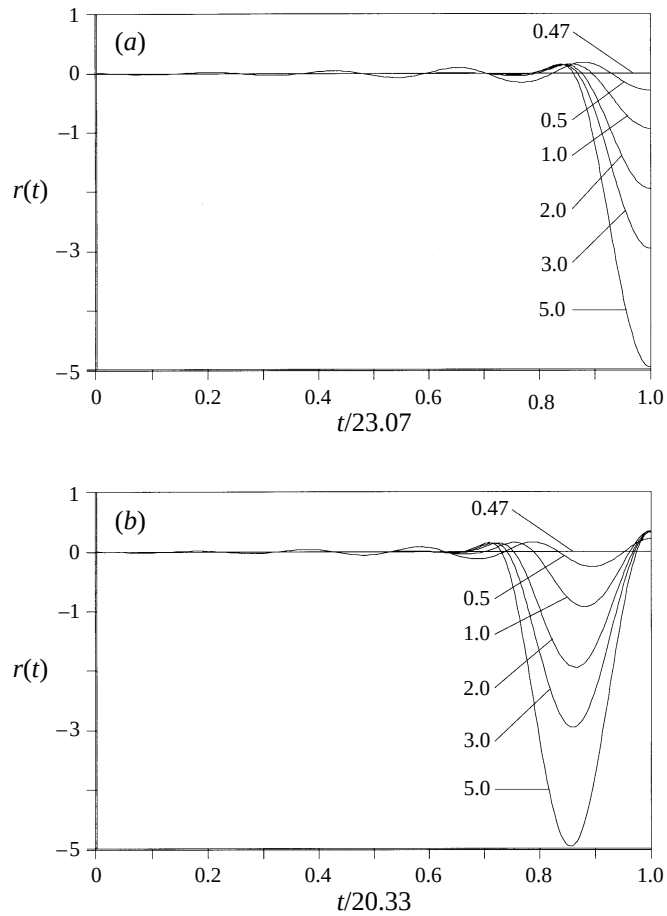

FIGURE 5. (*a*) Solutions on the primary branch for $b = -0.5$ and the given values of a; (*b*) solutions on the **2**(2) branch for the same parameter values.

with another branch; the labelling of the pairs of coalescing orbits is found to be the same as before. Further numerical experiments reveal that the behaviour of the **2**(2) branch changes for larger values of a. This difference is explained in detail in §5.2.

Figure 9 shows the results of numerical experiments in which bimodal waves are continued in a and b until limit points are reached; at these points the bimodal orbits coalesce with other multi-modal orbits. The dashed lines are the loci of such points. Observe that the curve of limit points for the **2**(n) waves, where n is odd, lies closer to C_2 for larger values of n; further numerical experiments indicate that this phenomenon continues as n increases. A similar accumulation of limit-point curves on C_2 is observed numerically for the **2**(n) waves, where n is even, the **2**(2) and **2**(4) waves being exceptions to this rule. For example, when $a = 1$ the **2**(6) and **2**(8) waves reach their limit points with respect to b at -0.670263 and -0.680774. (These branches are not depicted in figures 4, 8 or 9 in order to keep those diagrams uncluttered; the **2**(2) branch is also not shown in figure 9 for reasons explained in §5.2.) Note that a similar pattern involving separate accumulation of limit points corresponding to odd and even bi-modal solutions was found by Buffoni *et al.* (1996*a*) for equation

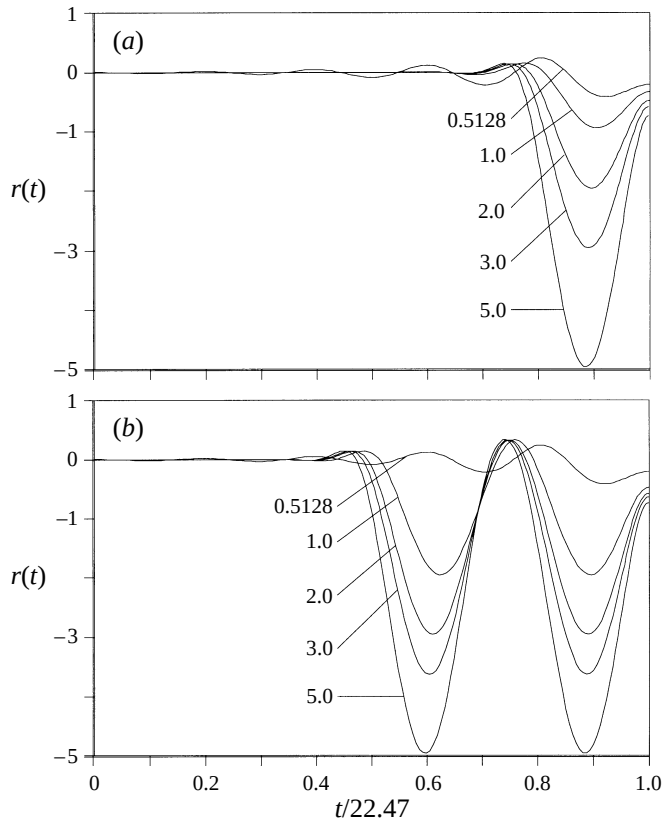

FIGURE 6. (*a*) Solutions on the **2**(1) branch for $b = -0.5$ and the given values of a up to the limit point at $a = 0.5128$; (*b*) solutions on the other branch coalescing at the limit point.

(1.8), who also gave a partial explanation in terms of the geometry of the stable and unstable manifolds.

The next step is to consider the situation when a is kept fixed and b is increased until one encounters the curve C_1 (at $b = (8/15)^{1/2}$ for $a = 1$). The behaviour in numerical experiments is observed to be the same as that described by the rigorous theory in §2.3. The primary solution survives as one crosses C_1; the eigenvalues become real, so that the tails of the wave become monotone (see figure 10*a*). The large troughs of all other solitary waves separate with increasing speed (see figure 10*b* for the **2**(2) branch). There are numerical difficulties in following branches of multi-modal solutions all the way back to $(8/15)^{1/2}$. These difficulties, reported by Champneys & Spence (1993), are connected with the fact that the speed of trough separation becomes infinite in the limit. Nevertheless, the numerical evidence strongly supports the hypothesis that the bifurcation phenomenon described in §2.3 occurs not only near the origin but whenever one crosses the curve C_1 from right to left. On the right of the curve C_1 the primary solution is connected as an open phenomenon to the solitary wave of depression that bifurcates from C_4 (see §2.1).

Notice that there are also asymmetric multi-modal solutions in the parameter regime. Figure 11 shows numerical computations of four tri-modal solitary waves (those labelled **3**(2,1), **3**(2,2), **3**(2,3) and **3**(2,4)) at $a = 1$, $b = -0.5$.

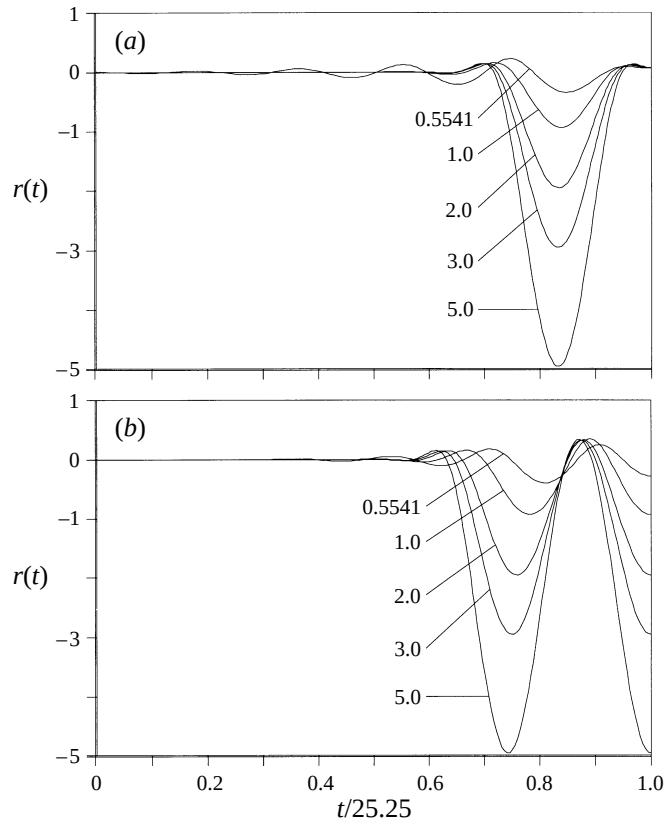

FIGURE 7. (*a*) Solutions on the **2**(4) branch for $b = -0.5$ and the given values of a up to the limit point at $a = 0.5541$; (*b*) solutions on the other branch coalescing at the limit point.

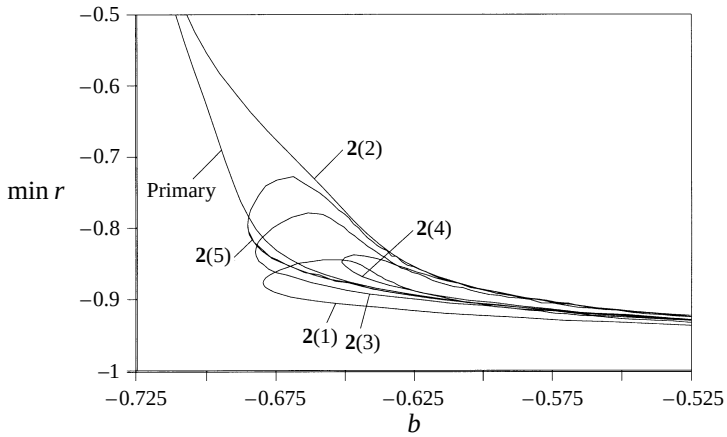

FIGURE 8. Bifurcation diagram with b of primary and five bi-modal solitary waves of depression for fixed $a = 1$. The jagged lines are an artifact of the numerical algorithm measuring the minimum of r; they do not indicate inaccuracies in the solution.

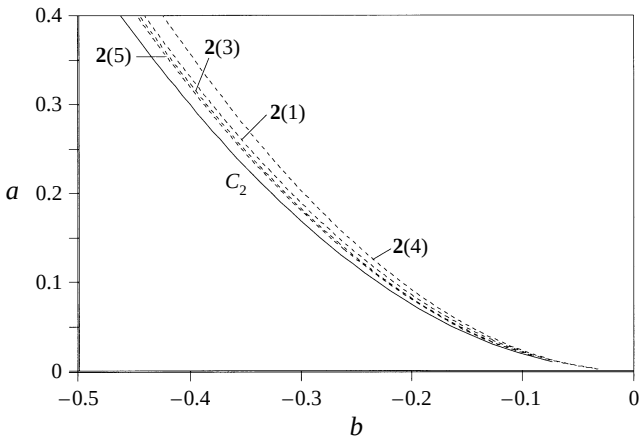

FIGURE 9. The dashed lines show loci of limit points of bimodal orbits; the solid line is the curve C_2.

Finally, turning to the full water-wave problem, let us remark that Dias, Menasce & Vanden-Broeck (1996) have found similar global existence properties for multi-modal solitary waves of depression; in particular they discovered a phenomenon similar to the coalescence between the **2**(1) and **4**(2,1,2) branches presented above.

4. Solitary waves of elevation – isolated solution branches

Let us begin by considering the reduced equation (1.4) in the case $a, b < 0$. Writing $a = -15b^2\mu/2$, where μ is a positive, real number, and introducing the scaled variables

$$u(T) = \frac{1}{5b^2\mu} r(t), \qquad T = \left(\frac{-15b\mu}{2}\right)^{1/2} t, \tag{4.1}$$

one obtains the equation

$$\mu u^{\mathrm{iv}} + \ddot{u} - u + u^2 = 0, \tag{4.2}$$

in which the dot denotes differentiation with respect to T. (Notice that (4.2) may also be obtained from the one-parameter equation (1.9) for $P > 0$ using the scaling

$$\mu = \frac{1}{P^2}, \quad U(T) = -u(t), \quad T = \left(\frac{1}{P}\right)^{1/2} t,$$

in which u and t denote the variables in (1.9).) The question of the existence of homoclinic solutions to (4.2) or (1.1) in the parameter region S_3 in figure 1 is an example of 'asymptotics beyond all orders': in order to determine whether a series approximating the solution converges one has to examine exponentially small terms (Kichenassamy & Olver 1992, §8). Hammersley & Mazzarino (1989), Amick & McLeod (1992) and Eckhaus (1992*a*, *b*) examined equation (4.2) and proved that it has no homoclinic solutions for sufficiently small values of μ. The existence of generalized solitary-wave solutions for sufficiently small values of μ has been established by Amick & Toland (1992*c*) (see also Hunter & Scheurle 1988 and Boyd 1991). These results apply to equation (1.9) for large, positive values of P and to equation (1.4) for small, negative values of a and negative values of b (the region S_3 in figure 1.)

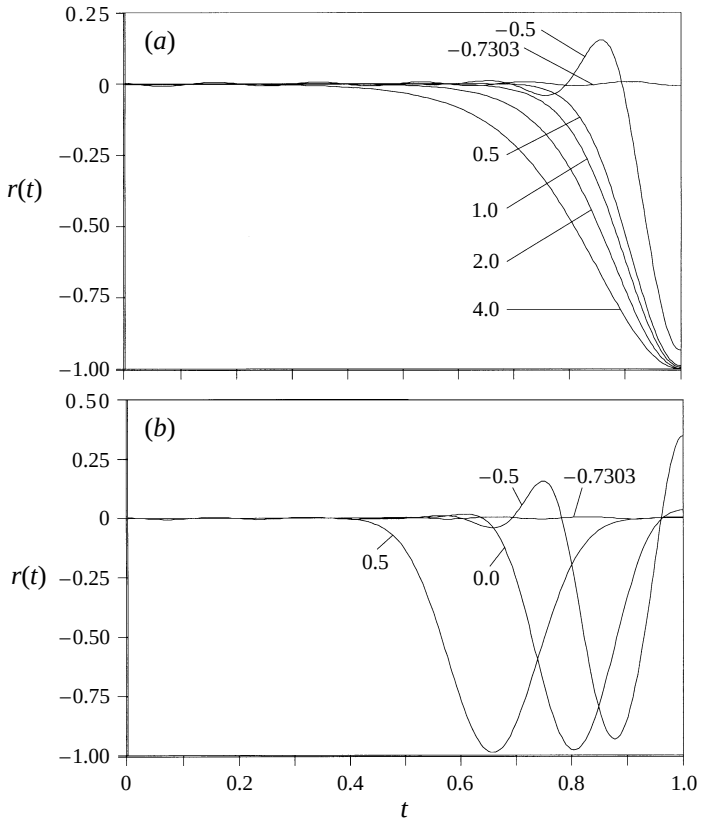

FIGURE 10. Solutions on (*a*) the primary; (*b*) the **2**(2) branch for $a = 1$ and the given values of b.

Equation (1.4) has also been studied for larger values of μ. Amick & McLeod (1992) showed that (4.2) has no symmetric homoclinic solution for any positive value of μ. For positive values of μ the linearized version of (4.2) has a saddle-centre, and it is known (Koltsova & Lerman 1995) that symmetric and asymmetric homoclinic solutions to such systems are respectively codimension-one and codimension-two phenomena. These facts lead one to conjecture that equation (4.2) has no homoclinic solution for any positive value of μ; Champneys & Lord (1997) present some numerical evidence to support this conjecture. (The main results of Champneys & Lord are computations of generalized solitary-wave solutions to (4.2) for larger values of μ, together with numerical evidence for multi-modal versions of these solutions which have a rich bifurcation structure.) Observe that these results apply to equation (1.9) for positive values of P and to equation (1.4) for negative values of a and b.

The above discussion indicates that to find homoclinic solutions to (1.1) in the parameter regime S_3 in figure 1 one has to study it in its original form as a two-parameter equation. Kichenassamy & Olver (1992) present a criterion for a general higher-order model equation to possess an explicit solution of the form $r(t) = \alpha \mathrm{sech}^2 \lambda t$. Using their criterion, one finds that

$$r(t) = 3\left(b + \tfrac{1}{2}\right) \mathrm{sech}^2\left(\left[\tfrac{3}{4}(2b+1)\right]^{1/2} t\right) \tag{4.3}$$

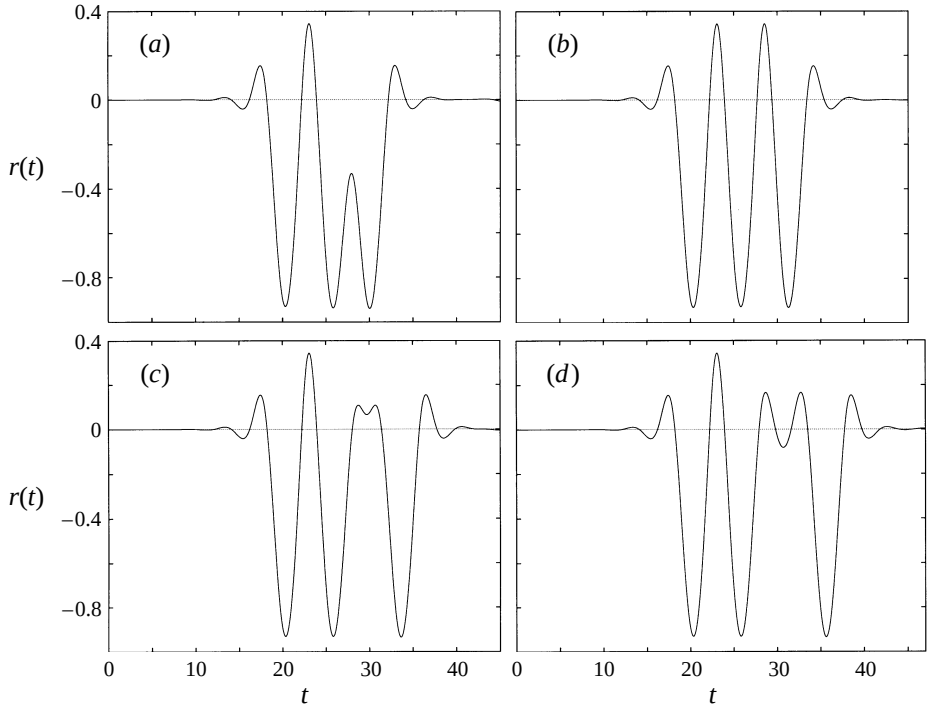

FIGURE 11. Four tri-modal solitary waves of depression for $a = 1$, $b = -0.5$: (*a*) **3**(2,1); (*b*) **3**(2,2); (*c*) **3**(2,3); (*d*) **3**(2,4).

defines an exact solution of (1.1) along the curve

$$a = \tfrac{3}{5}(2b+1)(b-2), \qquad b \geqslant -\tfrac{1}{2}. \tag{4.4}$$

Numerical experiments indicate that equations (4.3), (4.4) represent the first of a countable number of branches of homoclinic solutions to (1.1), the loci in the (b,a)-plane of which are parameterized by b. Each branch has the same qualitative features as the first (see figure 12). The nth branch B_n begins at $(b,a) = (b_n^-, 0)$ (with a bifurcation of a homoclinic orbit from the zero solution), reaches a turning point and enters the region $a > 0$ at $(b,a) = (b_n^+, 0)$. (Here $0 > b_1^- > b_2^- > \cdots$ and $0 < b_1^+ < b_2^+ < \cdots$.) Figure 13 shows numerical computations of the homoclinic solutions on the first few branches at $b = b_1^+$, b_2^+, b_3^+ and b_4^+. The solutions have the basic profile shown in figure 13(*a*) with an increasing number of small oscillations superimposed; they are all positive, symmetric and decay exponentially and monotonically to zero as $t \to \pm\infty$.

Recall that equation (1.4) has no homoclinic solutions in the present parameter regime. To show how this fact is consistent with the results of the numerical experiments in this section, let us briefly return to the scaled equation (1.6), to which the above calculations apply when $\epsilon = 1$. Figure 14 shows the effect of varying ϵ upon the solutions computed in figure 13; the values of b_n^- and b_n^+, $n = 1,2,3,4$, increase, as do the amplitudes of the solutions. Further numerical experiments indicate that the branches in figure 12(*a*) retain their qualitative shape as ϵ is decreased but become bigger, with larger values of b_n^- and b_n^+, $n = 1,2,3,4$. As $\epsilon \to 0$ one finds that b_n^-, b_n^+ and the amplitudes of the solutions tend to infinity. This behaviour is of course consistent with the fact that the limit equation (1.4) has no homoclinic solutions.

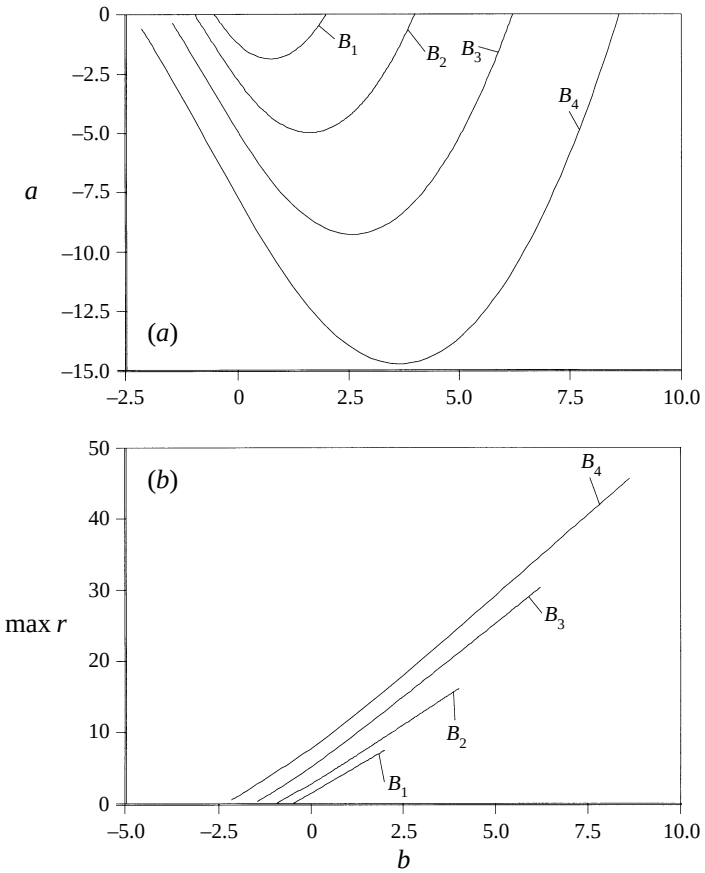

FIGURE 12. Bifurcation diagrams showing the branches B_1, B_2, B_3, B_4 of solitary waves of elevation for $a < 0$: (*a*) loci of branches in the (b, a)-plane; (*b*) maximum of r versus b.

5. Solitary waves of elevation – global phenomena

5.1. *Fast- and slow-decaying solitary waves*

Let us now return to equations (4.3) and (4.4), which define the branch B_1 of explicit solutions to equation (1.1). When $-1/2 < b < 2$ its locus lies in the region $a < 0$, where the linearized version of (1.1) has two real eigenvalues $\pm\lambda_1(a, b)$ and two purely imaginary eigenvalues $\pm\lambda_2(a, b)$. As b is increased through 2 the locus enters the region $\mathscr{R}$ above C_4 and to the left of C_1 in figure 1; the purely imaginary eigenvalues $\pm\lambda_2(a, b)$ decrease in magnitude to zero (when $b = 2$) and then become real with $|\lambda_2| < |\lambda_1|$. Observe that solitary waves on the branch decay exponentially to zero at infinity like $\exp(-|\lambda_1|t)$.

Homoclinic solutions to a Hamiltonian system whose linearization has four real eigenvalues $\pm\lambda_1$, $\pm\lambda_2$ with $|\lambda_2| < |\lambda_1|$ are open phenomena, but generically they decay exponentially to zero at infinity like $\exp(-|\lambda_2|t)$. For $b > 2$ equations (4.3), (4.4) therefore distinguish a branch of *fast-decaying solitary waves* (of elevation). Similar remarks apply to the other branches of solitary waves computed in §4. Figure 15 shows numerical computations of these branches; as one moves along each branch, the solutions grow in amplitude but retain the same qualitative wave shape. Recall that there are also generic *slow-decaying solitary waves* (of depression) in this region

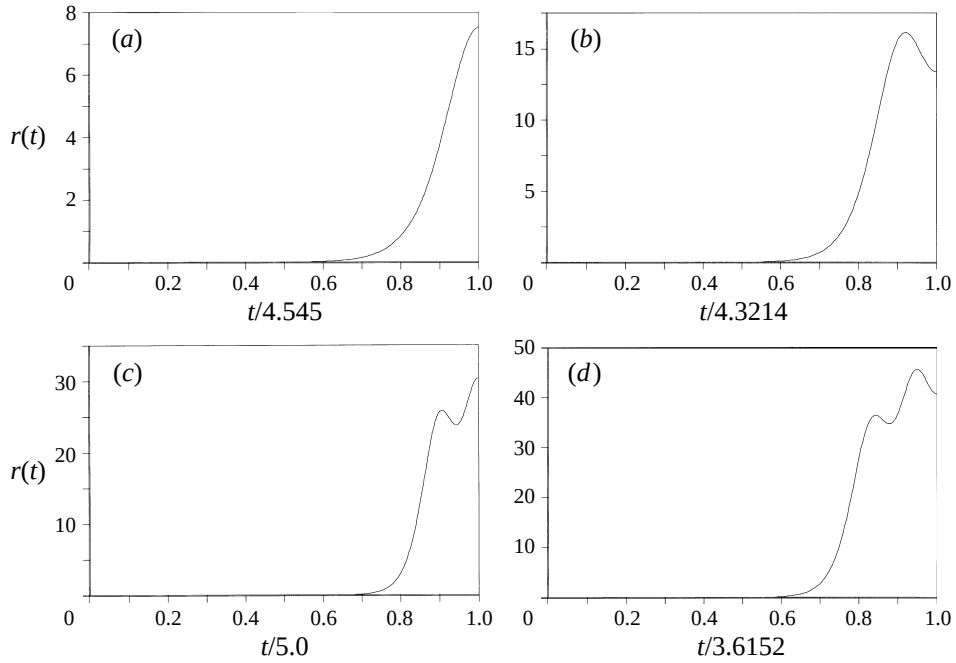

FIGURE 13. Solitary waves of elevation on the first four branches: (*a*) $(b,a) = (b_1^+, 0)$, where $b_1^+ = 2$; (*b*) $(b,a) = (b_2^+, 0)$, where $b_2^+ = 4.00571$; (*c*) $(b,a) = (b_3^+, 0)$, where $b_3^+ = 6.22095$; (*d*) $(b,a) = (b_4^+, 0)$, where $b_4^+ = 8.61990$.

which are associated with the bifurcation of the Korteweg–deVries solitary wave of depression discussed in §2.1. Varying a single parameter, one therefore expects to be able to follow a branch of generic, slow-decaying solitary waves through a branch of fast-decaying solitary waves. The generic solution on the former branch undergoes a codimension-one *orbit-flip bifurcation* (Sandstede 1993) as it passes through the latter branch. In general this bifurcation can take place either in the stable or in the unstable manifold. In the unstable manifold, an orbit-flip bifurcation occurs when the tail of the generic homoclinic solution flips from one direction to the opposite direction on the eigenvector corresponding to the smallest positive eigenvalue (figure 16). Similar remarks apply for the stable manifold. Note, however, that for symmetric homoclinic orbits in reversible systems orbit-flip bifurcations occur simultaneously in the stable and unstable manifolds.

Let us now verify the above remarks for equation (1.1) in the parameter regime $\mathscr{R}$. Figure 17 shows a branch of generic, slow-decaying solitary waves of elevation passing through the branch B_1 of fast-decaying solitary waves of elevation for fixed $a = 1$. Starting at $b = 4$, one may follow the branch of slow-decaying solitary waves through B_1 (at $b = (9 + (345)^{1/2})/12$) and then through the curve C_1 (at $b = (8/15)^{1/2}$) to enter the region $\mathscr{C}$ in figure 1. Here its tail becomes oscillatory (but still exponentially decaying) because of the change in eigenvalue structure. The branch reaches a limit point at $b = 0.108965$, turns, and crosses C_1 to enter the region $\mathscr{R}$ again. At $b = 0.108965$ one therefore observes a coalescence of two branches of solitary waves of elevation; numerical experiments indicate that both branches may be followed to arbitrarily large values of b. For future reference, let us refer to solutions on the first branch as type E_1 and those on the second as type E_2.

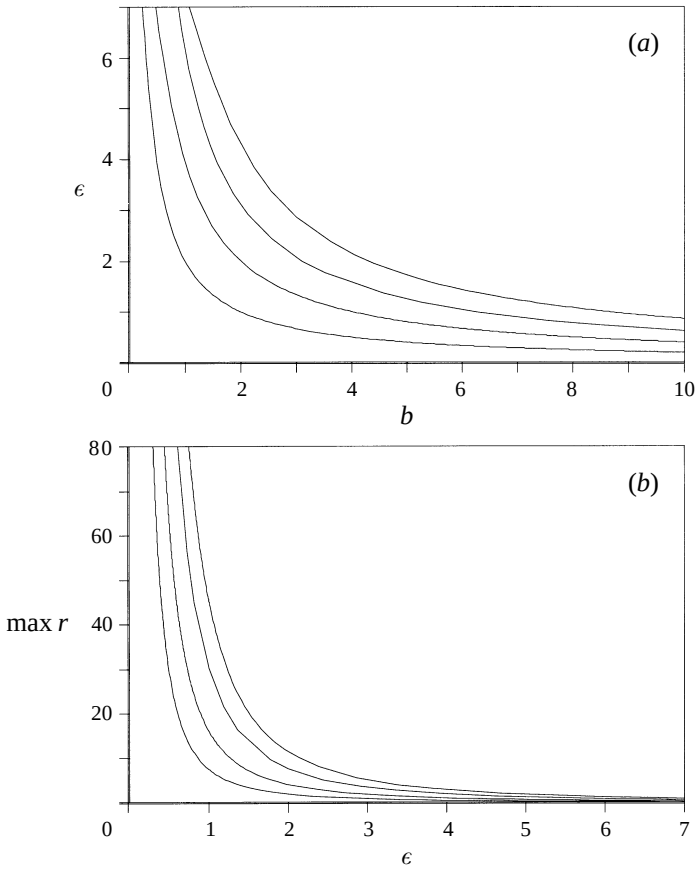

FIGURE 14. Behaviour of the first four branches at $b = b_1^+, b_2^+, b_3^+, b_4^+$ as ϵ varies: (*a*) ϵ versus b; (*b*) maximum of r versus ϵ.

Figure 18 is the analogue of figure 17 for a branch of generic, slow-decaying solitary waves of elevation passing through the branch B_2 of fast-decaying solitary waves of elevation. The observed behaviour is qualitatively the same as that of the first branch, except that it does not cross the curve C_1; the limit point is at $b = 2.49259$.

5.2. *Interactions with solitary waves of depression*

Figure 19 shows the result of a numerical experiment in which solitary waves of elevation of type E_1 are continued in a and b until a limit point is reached. The dashed line L is the locus of such limit points; note the cusp at $a = a_1 \approx 1.07$ and the local maximum to the right of the cusp at $a = a_2$. Limit points on the curve to the right of the cusp represent coalescences between solitary waves of type E_1 and E_2, as discussed in §5.1. To describe the phenomenon represented by limit points to the left of the cusp, it is necessary to recall some of the results in §3 concerning solitary waves of depression.

The numerical evidence in §3 indicates that the bifurcation phenomenon described in §2.3 occurs whenever one crosses the curve C_1 from right to left. Fixing a and allowing b to decrease through $(8a/15)^{1/2}$, one observes a slow decaying solitary wave of depression bifurcate into a plethora of multi-modal solitary waves of depression. When $a < a_1$ the bifurcation picture for $-(8a/15)^{1/2} < b < (8a/15)^{1/2}$ is as shown

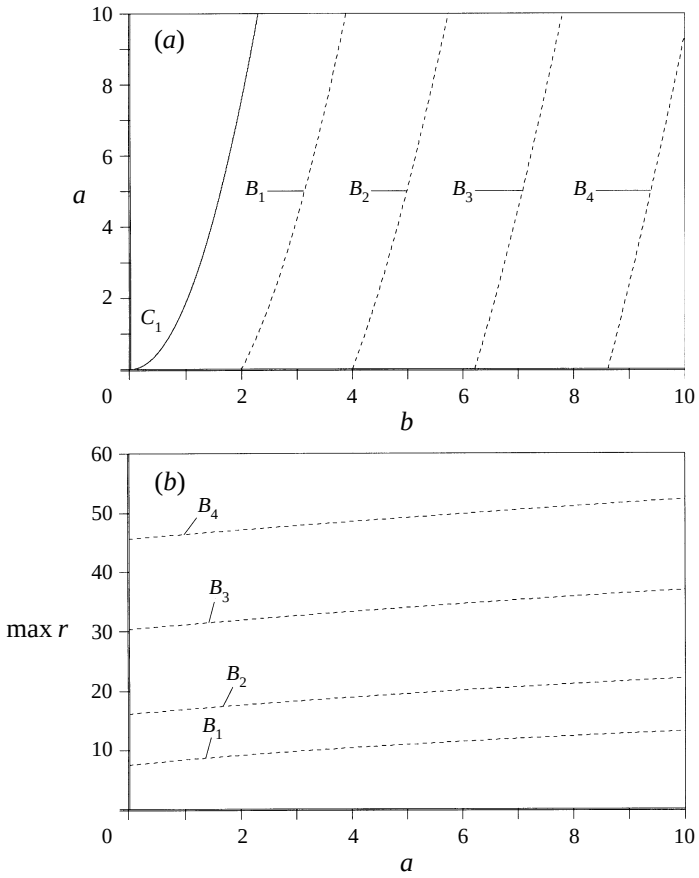

FIGURE 15. Branches of fast-decaying solitary waves of elevation for $a > 0$: (a) loci of branches together with the curve C_1 in (b, a)-parameter space; (b) maximum of r against a.

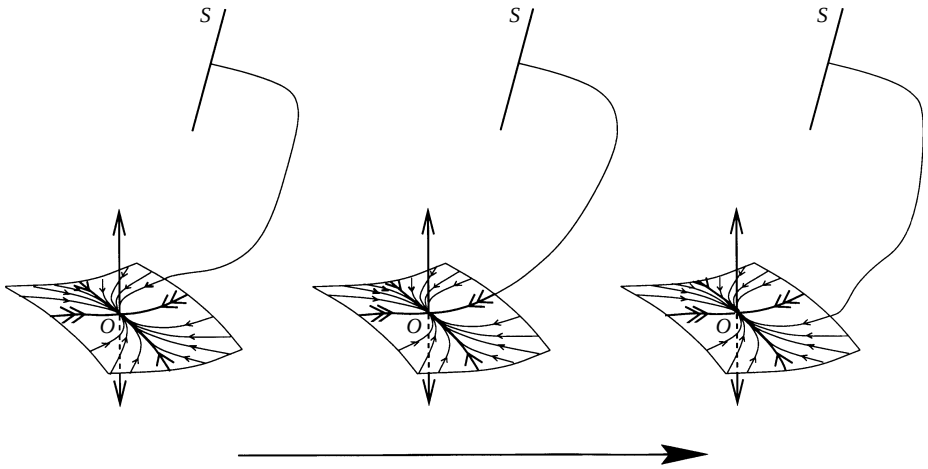

FIGURE 16. An orbit undergoing an orbit-flip bifurcation as a parameter is varied. The slow and fast directions are shown respectively by single and double arrows and S denotes the symmetric section.

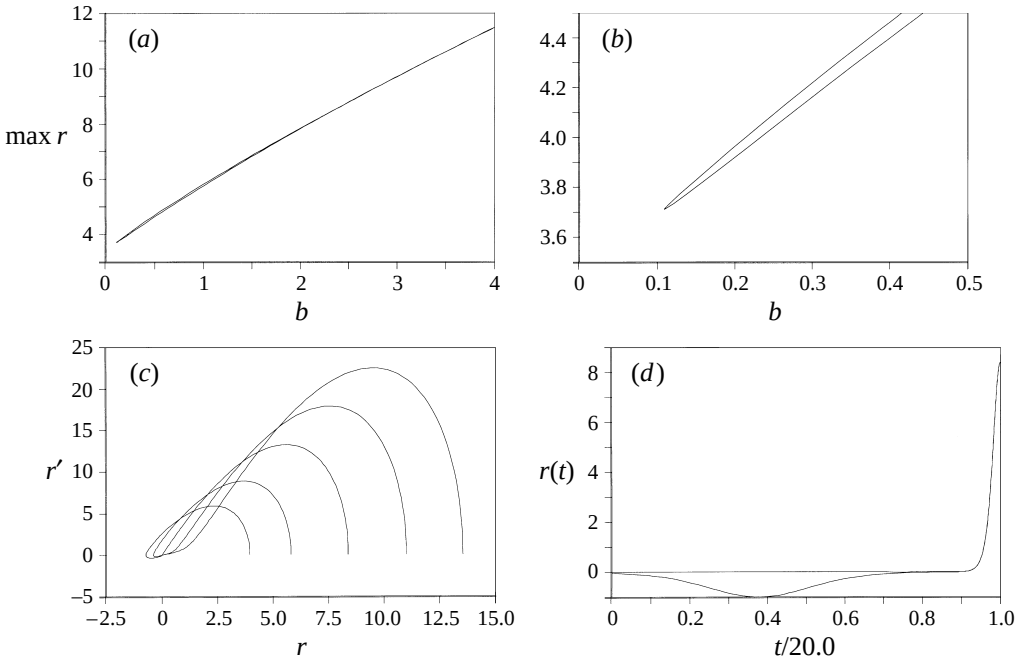

FIGURE 17. (*a*) Bifurcation diagram with b of a branch of solitary waves of elevation for fixed $a = 1$; (*b*) blow-up of (*a*) near the limit point; (*c*) the fast-decaying solution and four slow-decaying solutions for values of b near B_1; (*d*) the two solutions at $b = (9 + (345)^{1/2})/12$.

in Figure 8; all the branches of multi-modal solitary waves of depression coalesce in pairs with the exception of the primary and **2**(2) branches. Those branches connect with the branches of envelope solitary waves of elevation and depression which bifurcate from the zero solution at $b = -(8a/15)^{1/2}$. When $a > a_1$ the primary branch connects with the branch of envelope solitary waves of elevation as before. The **2**(2) branch, however, coalesces with the E_1 branch at its limit point, and the E_2 branch connects with the branch of envelope solitary waves of depression (figure 20).

Figure 19 shows there are three limit points with respect to b for $a \in (a_1, a_2)$. Figure 21 illustrates the results of numerical experiments to investigate how the **2**(2) and E_2 branches interchange as continuations of the enevlope solitary waves of depression bifurcating from zero at C_2. This unfolding is consistent with the theory of perturbed pitchfork bifurcations and hysteresis points (Golubitski & Schaeffer 1985, Chapter III).

5.3. *A plethora of solitary waves of elevation*

The fact that one can numerically follow the E_1 branch into the region $\mathscr{C}$ is strong evidence that orbits on this branch are transverse in the sense explained in §2.3. As in §2.3, one may then appeal to the theory by Devaney (1976) to obtain the existence of infinitely many multi-modal solitary waves. The overall structure of the set of these homoclinic solutions is the same as that of the set $\mathscr{H}$ described in §2.3; here, however, the solutions are waves of elevation. Bearing the numerical evidence in mind, one may conjecture that there are infinitely many multi-modal solitary waves of elevation in the region above L and to the left of C_1. Further numerical evidence for this conjecture is given in figure 22, which shows numerical computations of

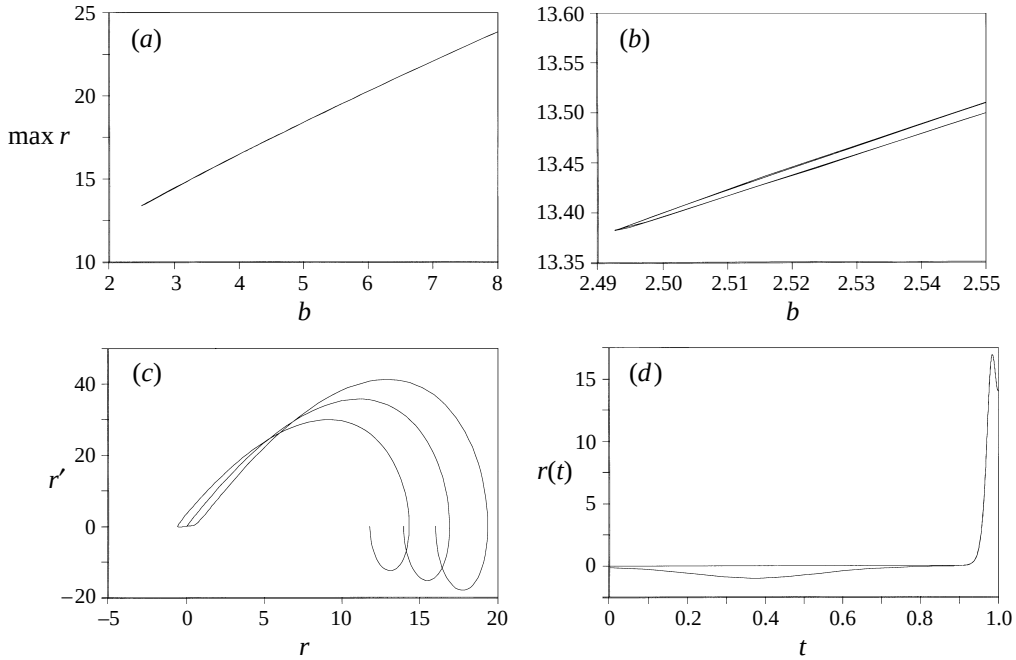

FIGURE 18. The analogue of figure 17 for a branch of slow-decaying solutions passing through the branch B_2 at $b = 4.23320$.

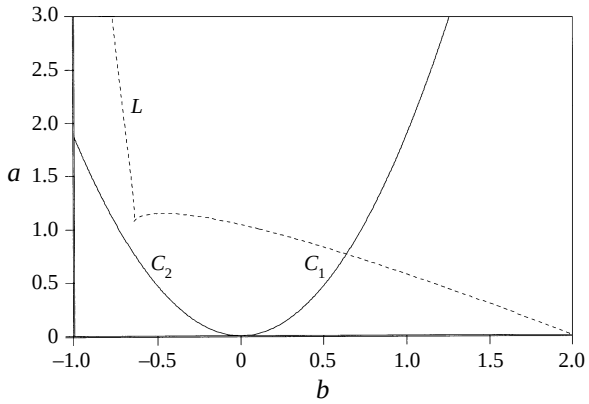

FIGURE 19. The dashed line L is the locus of limit points of E_1 solitary waves; the solid line is the curve $C_1 \cup C_2$.

the solution of type E_1 and four associated bi-modal waves of elevation at $a = 2$, $b = 0.5$. It should be possible to repeat the numerical experiments in §3 for the present multi-modal solitary waves of elevation; one would expect a bifurcation structure involving coalescences of branches at limit points. That investigation is, however, not undertaken here.

Observe that Devaney's result can be applied to any transverse homoclinic orbit in the region $\mathscr{C}$. For example, one would therefore expect to find multi-modal orbits that resemble multiple copies of solitary waves of type E_2.

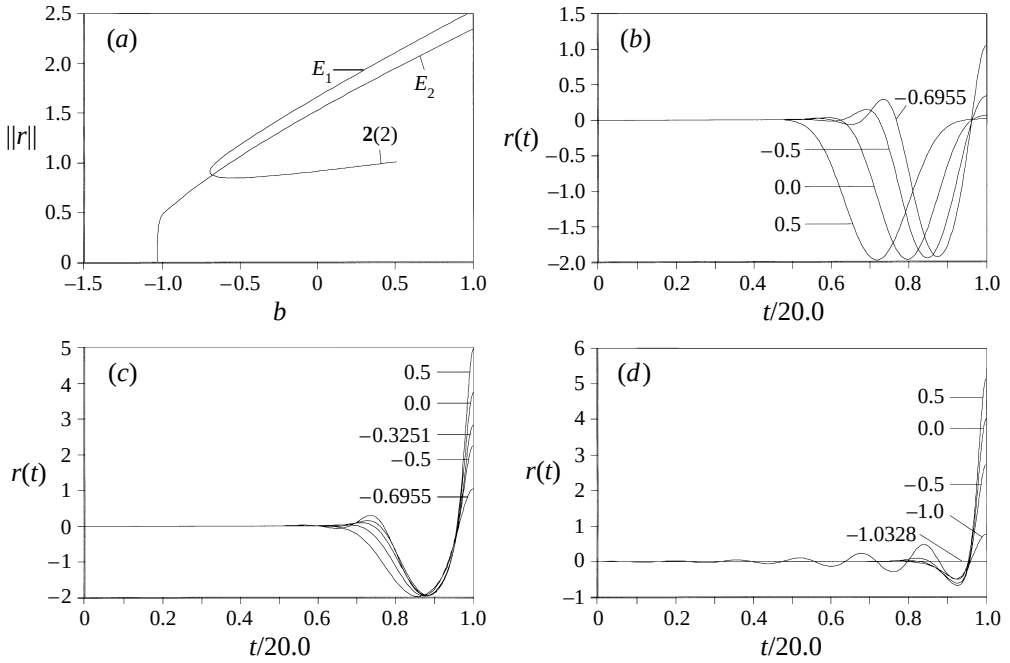

FIGURE 20. (*a*) Bifurcation diagram with b for fixed $a = 2$ showing the primary and **2**(2) branches of solitary waves of depression together with the E_1 branch of solitary waves of elevation, where $\| r \|$ is a scaled L^2-norm of the vector (r, r', r'', r'''); (*b*) solutions on the **2**(2) branch up to the limit point at $b = -0.6955$; (*c*) solutions on the E_1 branch, which coalesces with the **2**(2) branch at the limit point; (*d*) solutions on the E_2 branch.

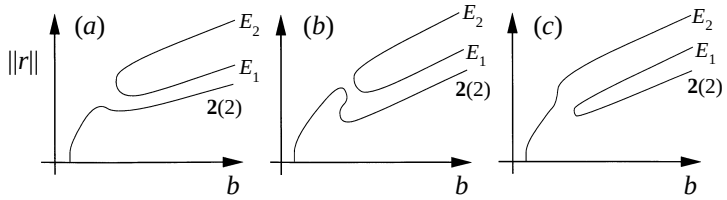

FIGURE 21. Schematic representation of bifurcation diagrams with b for (*a*) $a < a_1$; (*b*) $a_1 < a < a_2$; (*c*) $a > a_2$.

5.4. *Multi-crested solitary waves with non-oscillatory tails*

Sandstede, Jones & Alexander (1997) have recently developed the theory of orbit-flip bifurcations in reversible systems. Under the generic hypotheses that a transverse orbit passes through the fast direction with non-zero speed as a parameter is varied (figure 16) and that the orbit flip does not take place in the adjoint dynamical system, they showed that there are infinitely many multi-crested waves on one side of the fast-decaying branch that resemble 2, 3, ... copies of the primary orbit. In contrast to the multi-modal orbits associated with Devaney's construction (§§2.3 and 5.3), there is generally only one orbit for each $N > 1$. As it stands, the theory is not applicable to equation (1.1) since for Hamiltonian systems an orbit flip must take place in the dynamical system and its adjoint simultaneously (Sandstede *et al.* 1997, Remark 2.1). However, work is in progress upon a Hamiltonian version of the theory, and preliminary results indicate that in this case multi-crested waves are to be found

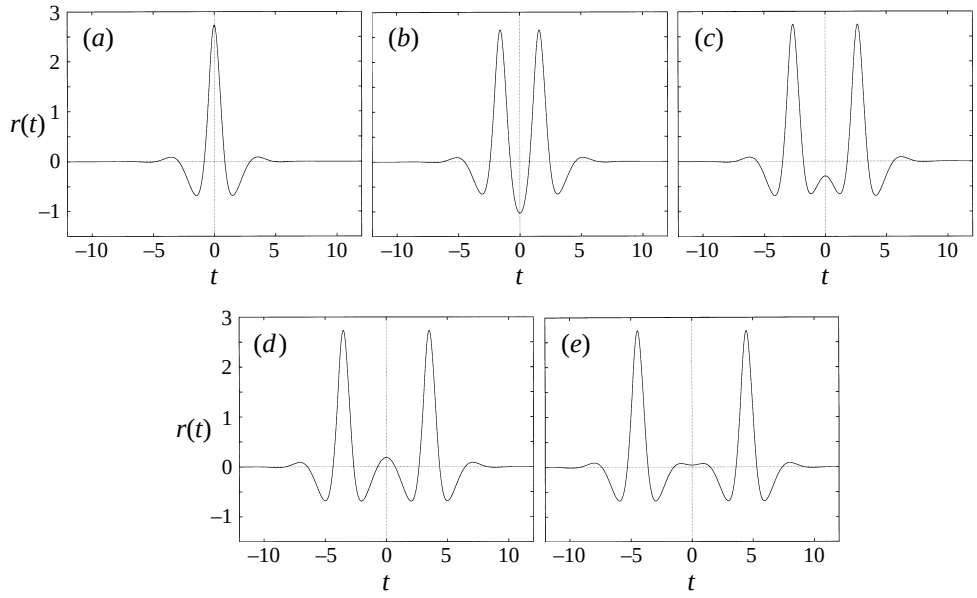

FIGURE 22. A solution of type E_1 as a primary orbit and four bi-modal waves of elevation at $a = 2$, $b = 0.5$: (*a*) primary; (*b*) **2**(2); (*c*) **2**(3); (*d*) **2**(4); (*e*) **2**(5).

either on both sides of the fast-decaying solution or not at all; the present system falls into the first category.

The above result is supported by numerical computations. Figure 23 depicts four solutions at parameter values to the left of B_1 in figure 15(*a*). These solutions resemble multiple copies of the primary solution associated with B_1 to the left of its orbit flip. Figure 24, on the other hand, depicts four solutions at parameter values to the right of B_1 but to the left of B_2. The first three resemble multiple copies of the primary solution associated with B_1 to the right of its orbit flip; note that, in contrast to the waves in figure 23, these solutions are strictly positive. The fourth solution (figure 24*d*) resembles two copies of the primary solution associated with B_2 to the left of its orbit flip; this solution does become negative.

Figures 25(*a*) and 25(*b*) show how the two-crested solutions shown in figures 23(*a*) and 24(*a*) change as the parameter b is varied; for $a = 3$ the orbit flip occurs at $b = (3 + (65)^{1/2})/4$. Both figures are consistent with a solution whose two large peaks move apart to infinity as an orbit flip is approached. Moreover, it is possible to continue the branch of solutions in figure 25(*b*) leftwards into the region $\mathscr{C}$ of complex eigenvalues. This fact suggests that the solution is transverse and that Devaney's theory applies to give infinitely many multi-modal solutions; these solutions resemble multiple copies of a two-crested primary wave separated by small oscillations and with oscillatory decaying tails.

6. Conclusion

A range of analytical and numerical results has been presented concerning the global bifurcation picture for homoclinic solutions to equation (1.1). The main features of these results are summarized in figure 26. The most surprising result is the strong evidence that there are infinitely many solitary waves for parameter values in the

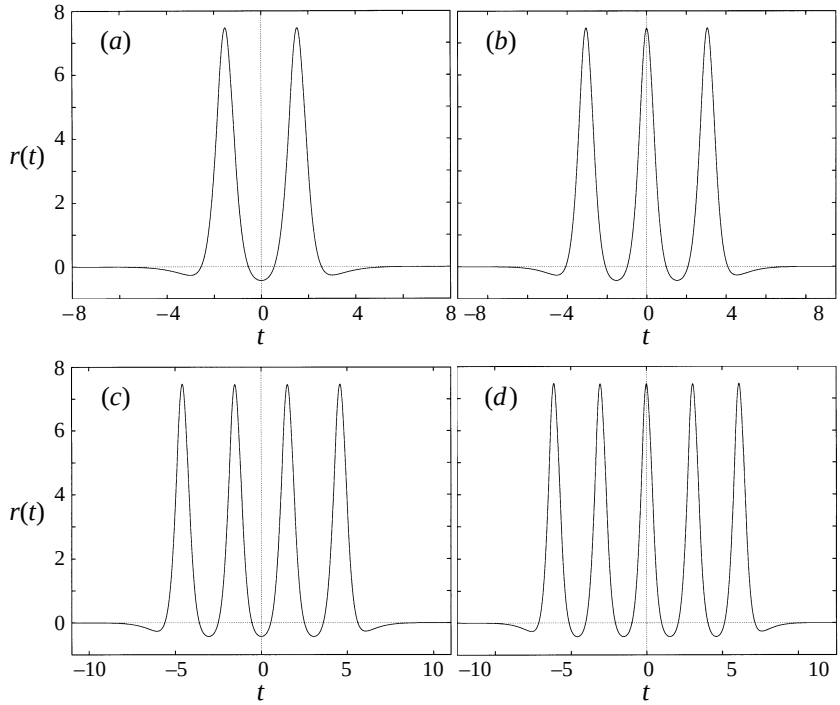

FIGURE 23. Four multi-modal waves of elevation for $a = 3.0$, $b = 1.5$.

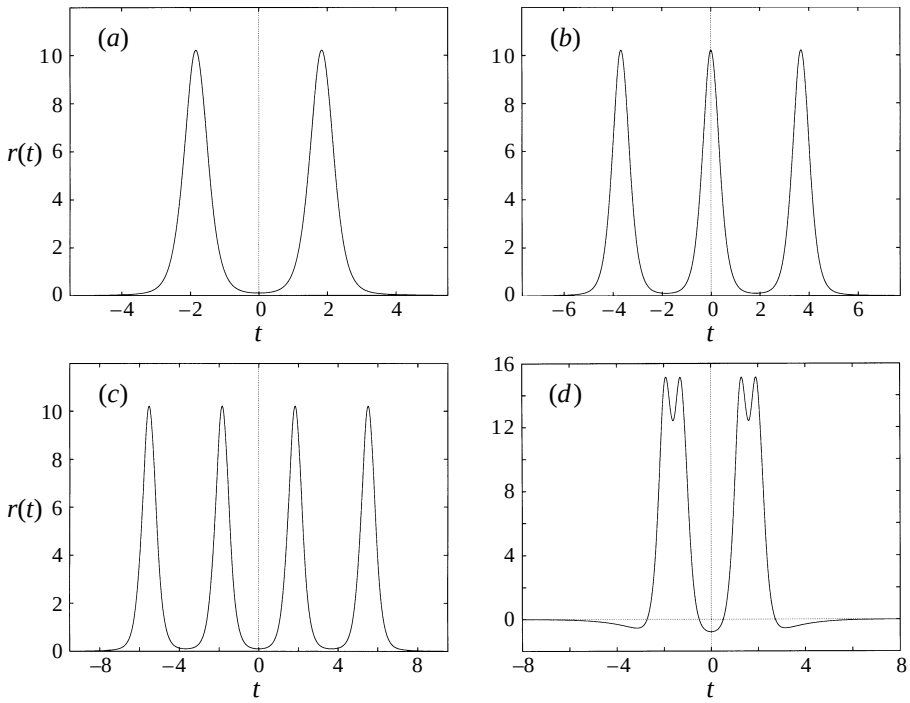

FIGURE 24. Four multi-modal waves of elevation for $a = 3.0$, $b = 3.0$.

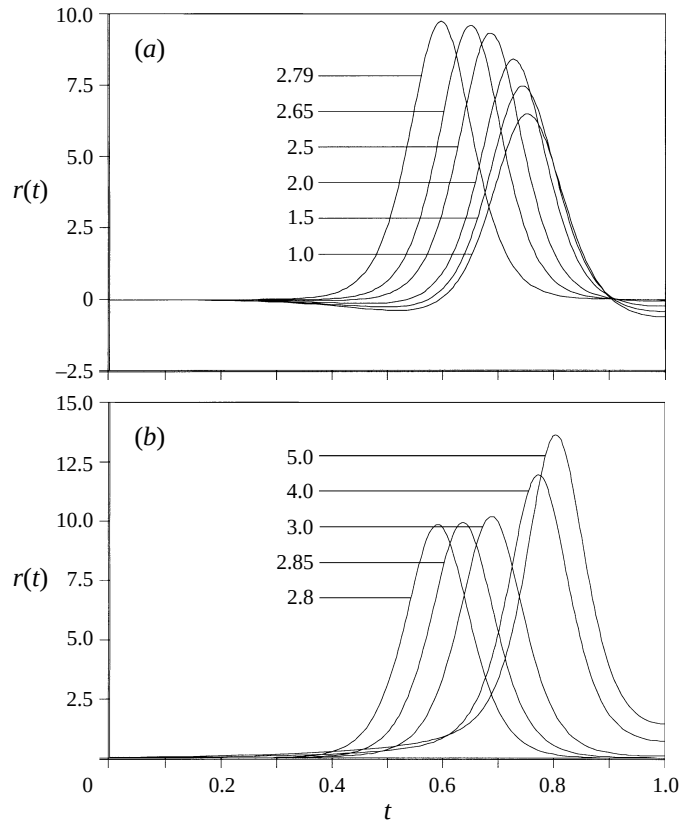

FIGURE 25. Solutions for $a = 3.0$ and the given values of b on branches of solitary waves including (a) that in figure 23(a); (b) that in figure 24(a).

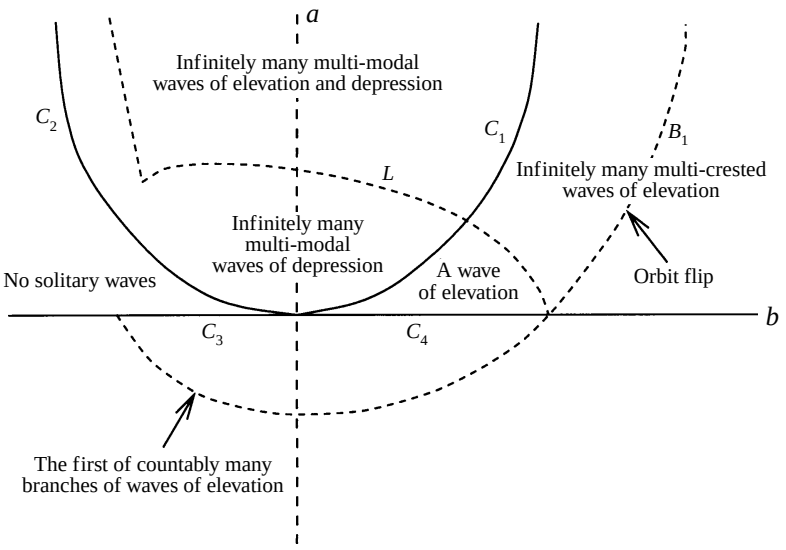

FIGURE 26. The main features of the conjectured global bifurcation diagram for solitary-wave solutions to the model equation. The curves C_1, C_2, C_3, C_4 correspond to those in figure 1. The boundary curves B_1 and L are discussed in detail in the text.

region $\mathscr{R}$ where there are four real eigenvalues; one would naturally expect uniqueness here (as Buffoni *et al.* 1996*a* prove for the simpler equation (1.8)). Let us also briefly mention a result by Holmes (1980), namely an existence theory for an infinite family of multi-bump homoclinic solutions in such a parameter regime. The central hypothesis in the theory is the existence of two distinct, slow-decaying homoclinic orbits whose asymptotic behaviour satisfies certain conditions; the solutions resemble multiple copies of these primary waves in an alternating sequence. To the right of B_1, the waves of type E_1 and the primary wave of depression found in §3.2 appear to be candidates for the primary waves in Holmes's theory, and the waves of type E_2 might arise as a consequence.

It remains to provide analytical results for some of the numerical evidence presented in this article. Transversality results are required for the application of Devaney's construction in several places, and delicate analysis is required to verify the example of 'asymptotics beyond all orders' described in §4. Work is in progress to obtain a rigorous theory for the orbit-flip phenomenon in §5.4.

An obvious issue not treated in this paper concerns the stability of the solitary waves as solutions of the partial differential equation (1.2). This issue has been addressed by Buryak & Champneys (1997) and Malomed & Vanden-Broeck (1996) for multi-modal solutions of the fifth-order KdV equation whose solitary waves solve (1.4). Buryak & Champneys considered the asymptotic limit of wide separation of the two troughs and showed that half the bi-modal solitary waves are stable and half unstable; Malomed & Vanden-Broeck showed numerically that the primary and simplest bi-modal waves can collide almost like solitons. Finally, Marchant & Smyth (1996) have recently presented numerical results concerning interactions between uni-modal solitary-wave solutions to a class of higher-order model equations.

This paper is dedicated to the memory of T. B. Benjamin FRS, who supervised us both when we were postgraduate students at the University of Oxford. We should like to thank Björn Sandstede (WIAS, Berlin) for explaining his results on orbit-flip bifurcations in reversible systems.

REFERENCES

Amick, C. J. & Kirchgässner, K. 1989 A theory of solitary water waves in the presence of surface tension. *Arch. Rat. Mech. Anal.* **105**, 1–49.

Amick, C. J. & McLeod, J. B. 1992 A singular perturbation problem in water waves. *Stability Appl. Anal. Continuous Media* **1**, 127–148.

Amick, C. J. & Toland, J. F. 1992*a* Global uniqueness of homoclinic orbits for a class of 4th order equations. *Z. Angew. Math. Phys.* **43**, 591–597.

Amick, C. J. & Toland, J. F. 1992*b* Homoclinic orbits in the dynamic phase-space analogy of an elastic strut. *Eur. J. Appl. Maths* **3**, 97–114.

Amick, C. J. & Toland, J. F. 1992*c* Solitary waves with surface tension I: Trajectories homoclinic to periodic orbits in four dimensions. *Arch. Rat. Mech. Anal.* **118**, 37–69.

Beale, J. T. 1991 Solitary water waves with capillary ripples at infinity. *Commun. Pure Appl. Maths* **64**, 211–257.

Belyakov, L. A. & Shilnikov, L. P. 1990 Homoclinic curves and complex solitary waves. *Selecta Mathematica Sovietica* **9**, 219–228.

Benjamin, T. B. 1982 The solitary wave with surface tension. *Q. Appl. Maths* **40**, 231–234.

Boyd, J. 1991 Weakly non-local solitons for capillary-gravity water waves: fifth-order Korteweg-deVries equation. *Physica* D **48**, 129–146.

Brezis, H. & Nirenberg, L. 1991 Remarks on finding critical points. *Commun. Pure. Appl. Maths* **44**, 939–963.

Buffoni, B. 1993 Cascades of homoclinic orbits for Hamiltonian systems: further properties. *Nonlinearity* **6**, 1091–1092.

Buffoni, B. 1995 Infinitely many large-amplitude homoclinic orbits for a class of autonomous Hamiltonian systems. *J. Diffl Equat.* **121**, 109–120.

Buffoni, B. 1996 Periodic and homoclinic orbits for Lorenz-Lagrangian systems via variational methods. *Nonlinear Anal. Theory, Meth. Appl.* **26**, 443–462.

Buffoni, B., Champneys, A. R. & Toland, J. F. 1996*a* Bifurcation and coalescence of a plethora of homoclinic orbits for a Hamiltonian system. *J. Dyn. Diffl Equat.* **8**, 221–279.

Buffoni, B. & Groves, M. D. 1996 A multiplicity result for solitary gravity-capillary waves in deep water via critical-point theory. Preprint. (Available by anonymous ftp from *ftp.maths.bath.ac.uk: pub/preprints*.)

Buffoni, B., Groves, M. D. & Toland, J. F. 1996*b* A plethora of solitary gravity-capillary water waves with nearly critical Bond and Froude numbers. *Phil. Trans. R. Soc. Lond.* A **354**, 575–607.

Buffoni, B. & Séré, E. 1996 A global condition for quasi-random behaviour in a class of conservative systems. *Commun. Pure Appl. Maths* **49**, 285–305.

Buryak, A. V. & Champneys, A. R. 1997 On the stability of solitary wave solutions of the 5th order KdV equation. *Phys. Lett.* A (in press).

Champneys, A. R. & Lord, G. 1997 Computation of homoclinic solutions to periodic orbits in a reduced water-wave problem. *Physica* D **102**, 101–124.

Champneys, A. R. & Spence, A. 1993 Hunting for homoclinic orbits in reversible systems: a shooting technique. *Adv. Comput. Maths* **1**, 81–108.

Champneys, A. R. & Toland, J. F. 1993 Bifurcation of a plethora of multi-modal homoclinic orbits for autonomous Hamiltonian systems. *Nonlinearity* **6**, 665–722.

Coti Zelati, V., Ekeland, I. & Séré, E. 1990 A variational approach to homoclinic orbits in Hamiltonian systems. *Math. Ann.* **288**, 133–160.

Craig, W. & Groves, M. D. 1994 Hamiltonian long-wave approximations to the water-wave problem. *Wave Motion* **19**, 367–389.

Devaney, R. L. 1976 Homoclinic orbits in Hamiltonian systems. *J. Diffl Equat.* **21**, 431–438.

Dias, F. & Iooss, G. 1993 Capillary-gravity solitary waves with damped oscillations. *Physica* D **65**, 399–423.

Dias, F., Menasce, D. & Vanden-Broeck, J.-M. 1996 Numerical study of capillary-gravity solitary waves. *Eur. J. Mech. Fluids* B **15**, 17–36.

Doedel, E., Keller, H. B. & Kernevez, J. P. 1991 Numerical analysis and control of bifurcation problems. *Intl J. Bifurcation Chaos* **1**, 493–520, 745–772.

Doedel, E. & Kernevez, J. P. 1986 AUTO: Software for continuation problems in ordinary differential equations with applications. *California Institute of Technology, Applied Mathematics Tech. Rep.*

Eckhaus, W. 1992*a* On water waves at Froude number slightly higher than one and Bond number less than 1/3. *Z. Angew. Math. Phys.* **43**, 254–269.

Eckhaus, W. 1992*b* Singular perturbations of homoclinic orbits in $\mathbb{R}^4$. *SIAM J. Math. Anal.* **23**, 1269–1290.

Elphick, C., Tirapegui, E., Brachet, M. E., Coullet, P. & Iooss, G. 1987 A simple global characterization for normal forms of singular vector fields. *Physica* D **29**, 95–127.

Golubitski, M. & Schaeffer, D. G. 1985 *Singularities and Groups in Bifurcation Theory,* vol 1. Springer.

Grimshaw, R., Malomed, B. & Benilov, E. 1994 Solitary waves with damped oscillatory tails: an analysis of the fifth-order Korteweg-deVries equation. *Physica* D **77**, 473–485.

Groves, M. D. & Toland, J. F. 1997 On variational formulations for steady water waves. *Arch. Rat. Mech. Anal.* (in press).

Hammersley, J. M. & Mazzarino, G. 1989 Computational aspects of some autonomous differential equations. *Proc. R. Soc. Lond.* A **424**, 19–37.

Holmes, P. J. 1980 Periodic, nonperiodic and irregular motions in a Hamiltonian system. *Rocky Mountain J. Maths* **10**, 382–404.

Hunt, G. W., Bolt, H. M. & Thompson, J. M. T. 1989 Structural localisation phenomena and the dynamical phase-space analogy. *Proc. R. Soc. Lond.* A **425**, 245–267.

HUNT, G. W. & WADEE, M. K. 1991 Comparative Lagrangian formulations for localised buckling. *Proc. R. Soc. Lond.* A **434**, 485–502.

HUNTER, J. K. & SCHEURLE, J. 1988 Existence of perturbed solitary wave solutions to a model equation for water waves. *Physica* D **32**, 253–268.

IOOSS, G. 1992 A codimension 2 bifurcation for reversible vector fields. In *Proc. Workshop on Normal Forms*. Fields Institute.

IOOSS, G. 1995 Capillary-gravity water-waves problem as a dynamical system. In *Structure and Dynamics of Nonlinear Waves in Fluids* (ed. A. Mielke & K. Kirchgässner), pp. 42–57. World Scientific.

IOOSS, G. & ADELMEYER, M. 1992 *Topics in Bifurcation Theory and Applications*. World Scientific.

IOOSS, G. & KIRCHGÄSSNER, K. 1990 Bifurcation d'ondes solitaires en présence d'une faible tension superficielle. *C. R. Acad. Sci. Paris* (I) **311**, 265–268.

IOOSS, G. & KIRCHGÄSSNER, K. 1992 Water waves for small surface tension: an approach via normal form. *Proc. R. Soc. Edin.* A **122**, 267–299.

IOOSS, G. & PÉROUÈME, M. C. 1993 Perturbed homoclinic solutions in reversible 1:1 resonance vector fields. *J. Diffl Equat.* **102**, 62–88.

KICHENASSAMY, S. & OLVER, P. J. 1992 Existence and nonexistence of solitary wave solutions to higher-order model evolution equations. *SIAM J. Math. Anal.* **23**, 1141–1166.

KIRCHGÄSSNER, K. 1988 Nonlinear resonant surface waves and homoclinic bifurcation. *Adv. Appl. Maths* **26**, 135–181.

KNOBLOCH, J. 1994 Bifurcation of degenerate homoclinics in reversible and conservative systems. Technische Universität Illmenau, Preprint No. M 15/94.

KOLTSOVA, O. & LERMAN, L. M. 1995 Periodic orbits and homoclinic orbits in a two-parameter unfolding of a Hamiltonian system with a homoclinic orbit to a saddle-center. *Intl J. Bifurcation Chaos* **5**, 397–408.

KORTEWEG, D. J. & DEVRIES, G. 1895 On the change of form of long waves advancing in a rectangular channel, and on a new type of long stationary waves. *Phil. Mag.* (5) **39**, 422–443.

LOMBARDI, E. 1995 Exponential estimate of oscillations for generalized solitary waves. In *Structure and Dynamics of Nonlinear Waves in Fluids* (ed. A. Mielke & K. Kirchgässner), pp. 307–315. World Scientific.

MALOMED, B. & VANDEN-BROECK, J.-M. 1996 Solitary wave interactions for the fifth order KdV equation. *Contemp. Maths* **200**, 133–143.

MARCHANT, T. R. & SMYTH, N. F. 1996 Soliton interaction for the extended Korteweg-deVries equation. *IMA J. Appl. Maths* **56**, 157–176.

MEYER, K. A. & HALL, G. R. 1992 *Introduction to Hamiltonian dynamics and the N-body problem*. Springer.

SANDSTEDE, B. 1993 Verzweigungstheorie homokliner Verdopplungen. Doctoral thesis, Universität Stuttgart.

SANDSTEDE, B., JONES, C. K. R. T. & ALEXANDER, J. C. 1997 Existence and stability of N-pulses on optical fibers with phase-sensitive amplifiers. *Physica* D (in press).

SUN, S. M. 1991 Existence of a generalized solitary wave solution for water waves with positive bond number less than 1/3. *J. Math. Anal. Appl.* **156**, 533–566.

WIGGINS, S. 1988 *Global Bifurcations and Chaos: Analytical Methods*. Springer.

ZUFIRIA, J. 1987 Symmetry breaking in periodic and solitary gravity-capillary waves on water of finite depth. *J. Fluid Mech.* **184**, 183–206.